

MOLPHARM/2005/18556

**Zinc and mercuric ions distinguish mouse TRESK from the other two-pore-domain K<sup>+</sup> channels**

*GÁBOR CZIRJÁK AND PÉTER ENYEDI*

*Department of Physiology, Semmelweis University, Budapest, Hungary*

MOLPHARM/2005/18556

### Running title page

Running title: Mouse TRESK is inhibited by Zn<sup>2+</sup> and Hg<sup>2+</sup>

Key words: TRESK, KCNK, 2P, Mercury, Ruthenium Red, Zinc

Corresponding author:

Péter Enyedi, MD, PhD

Department of Physiology

Semmelweis University

P.O. Box 259, Budapest, Hungary, H-1444

Phone: (36-1-) 266-2755/4079

Fax: (36-1-) 266-6504

E-mail: enyedi@puskin.sote.hu

Number of text pages: 37

Number of tables: 2

Number of figures: 8

Number of references: 40

Number of words in the *Abstract*: 250

Number of words in the *Introduction*: 744

Number of words in the *Discussion*: 1489

Non-standard abbreviations: 2PK<sup>+</sup> channel: two-pore-domain K<sup>+</sup> channel, RR: ruthenium red

## ABSTRACT

TRESK is the most recently cloned two-pore-domain potassium ( $2\text{PK}^+$ ) channel, regulated by the calcium/calmodulin-dependent protein phosphatase, calcineurin. Functional identification of endogenous TRESK and its distinction from the other  $2\text{PK}^+$  channels, producing similar background  $\text{K}^+$  current, are impeded by the lack of specific inhibitors. Therefore, we searched for antagonists, selective against TRESK among the mouse  $2\text{PK}^+$  channels, by screening more than 200 substances. Mibefradil, zinc and mercuric ions inhibited TRESK, expressed in *Xenopus laevis* oocytes, with  $\text{IC}_{50}$  values below 10  $\mu\text{M}$ . The specificity of the identified agents was determined by measuring their effects on mouse TALK-1, TASK-1, TASK-2, TASK-3, THIK-1, TRAAK, TREK-1 and TREK-2. Mibefradil failed to discriminate well among the functional  $2\text{PK}^+$  channels, however,  $\text{Zn}^{2+}$  and  $\text{Hg}^{2+}$  exerted significantly stronger inhibitory effect on TRESK than on the other channels. Sensitivity to zinc, but insensitivity to ruthenium red were distinctive features of TRESK. Whereas both  $\text{Zn}^{2+}$  and  $\text{Hg}^{2+}$  were selective blockers of TRESK among the mouse  $2\text{PK}^+$  channels, human TRESK was resistant to  $\text{Zn}^{2+}$ , it was blocked only by  $\text{Hg}^{2+}$ . Histidine 132 of mouse TRESK was partly responsible for this difference. Mouse TRESK expressed in COS-7 cells was also inhibited by  $\text{Zn}^{2+}$  and  $\text{Hg}^{2+}$ , and TRESK single channel current was diminished in outside-out patches, indicating that the action of the ions was membrane delimited, most probably targeting the channel itself. Thus both  $\text{Zn}^{2+}$  and  $\text{Hg}^{2+}$  are expected to inhibit endogenous TRESK in isolated mouse cells, and these ions can be applied to identify the calcineurin-activated  $2\text{PK}^+$  channel in its natural environment.

## INTRODUCTION

The high resting potassium conductance of the plasma membrane is established by background (leak)  $K^+$  channels in several excitable and non-excitable cell types. These background channels belong to the family of two-pore-domain  $K^+$  (2PK<sup>+</sup>) channels, and their regulation by distinct physicochemical parameters and intracellular signaling mechanisms has been reported to contribute essentially to cell function (for reviews see Bayliss *et al.*, 2003 and Goldstein *et al.*, 2001). Their widespread expression and functional importance urge the more detailed investigation of background  $K^+$  currents in other cell types, however, the routine electrophysiological identification of two-pore-domain  $K^+$  channels is still considerably impeded by the lack of specific inhibitors.

The mammalian 2PK<sup>+</sup> channel family consists of 15 subunits divided into 6 subfamilies: TWIK, TASK, TREK, TALK, THIK and TRESK. Dimers of these subunits constitute the functional channels. In most cases this means homodimer formation, and heterodimerization has been reported only for one particular subunit combination (TASK-1/TASK-3) (Czirják and Enyedi, 2002). Members of the distinct subfamilies have strikingly different regulatory properties, but in general, standard whole-cell patch clamp recording does not allow their unequivocal identification. Although the different 2PK<sup>+</sup> channels exert a similar stabilizing effect on the resting membrane potential, it is obviously of central importance for the cell, whether this effect is achieved by pH-sensitive TASK (Talley *et al.*, 2000), mechanosensitive TREK (Maingret *et al.*, 2000), calcineurin-activated TRESK (Czirják *et al.*, 2004) or by some other 2PK<sup>+</sup> channels which have their own particular way of regulation.

Formerly, we reported that ruthenium red inhibited TASK-3 (and TRAAK, a member of

TREK subfamily), but not TASK-1. This observation provided the essential pharmacological tool to demonstrate TASK-1/TASK-3 heteromerization (Czirják and Enyedi, 2002). Since that time, ruthenium red has been applied to examine the distribution of TASK subfamily members and their heteromerization also in native cells (Berg *et al.*, 2004; Lauritzen *et al.*, 2003; Kang *et al.*, 2004a; Larkman and Perkins, 2005). Despite of the overall non-selectivity of ruthenium red (e.g. it inhibits voltage-dependent calcium channels as well as the mitochondrial calcium uniporter), this compound turned out to be a valuable tool in the investigation of  $2\text{PK}^+$  channels.

In the present study we describe the aimed search for TRESK (Twik-RElated Spinal cord  $\text{K}^+$  channel) inhibitors. Our primary goal was to find substances being selective for TRESK among the mouse  $2\text{PK}^+$  channels, and not necessarily presenting overall selectivity. These inhibitors may modify several other ion transport mechanisms in addition to TRESK, and thus care must be taken, when they are applied in complex functional studies. However, because of their specificity within the  $2\text{PK}^+$  channel family, they should be suitable for the analysis of the composition of background  $\text{K}^+$  currents, and consequently for the identification of TRESK in cells expressing the channel endogenously.

Endogenous TRESK mRNA expression was reported in the human spinal cord (Sano *et al.*, 2003; Liu *et al.*, 2004). We cloned TRESK also from mouse (AY325301), and demonstrated its mRNA to be expressed in cerebrum, cerebellum, brain stem, spinal cord and testicular tissue by RT-PCR (Czirják *et al.*, 2004). Simultaneously, mouse TRESK (with identical sequence, NM207261) was cloned also by another group (Kang *et al.*, 2004b), and named TRESK-2. In that study, high expression of TRESK was detected in rat thymus and spleen by Northern blot. Although human and mouse TRESK channels show low similarity (67%) at the amino acid level, the sequence of human “TRESK-2” or mouse “TRESK-1” has not been reported (and has not

been found by us in the human or mouse genome, respectively). Therefore in the present study we use our original denominations: human TRESK (hTRESK) and mouse TRESK (mTRESK).

Human and mouse TRESK, expressed in *Xenopus* oocytes, are regulated in a unique manner among the  $2\text{PK}^+$  channels. The cytoplasmic calcium signal induces maintained (several minutes long) and strong (5-10-fold) stimulation of TRESK current, through the activation of the  $\text{Ca}^{2+}$ /calmodulin-dependent protein phosphatase, calcineurin (Czirják *et al.*, 2004). By this regulation, cells expressing TRESK are expected to respond with maintained hyperpolarization and reduction of excitability to a single cytoplasmic calcium signal. The capability to store the memory of a foregoing calcium signal renders TRESK particularly interesting, and the identification of endogenous TRESK may facilitate further studies and shed light on the functional role of calcium-mediated background  $\text{K}^+$  current regulation in different cell types. With the present work we open up the way for these investigations by demonstrating that mouse TRESK can be discriminated from the other  $2\text{PK}^+$  channels, based on its high sensitivity to zinc and mercuric ions.

## **MATERIALS AND METHODS**

### **Materials**

Enzymes and kits for molecular biological studies were purchased from Ambion (Austin TX), Amersham (Little Chalfont, United Kingdom), Fermentas (Vilnius, Lithuania), New England Biolabs (Beverly, MA), Pharmacia Biotech (Uppsala, Sweden), Promega (Madison, WI), Qiagen (Valencia, CA) and Stratagene (La Jolla, CA). Fine chemicals of analytical grade were obtained from Fluka (Buchs, Switzerland), Promega and Sigma Chemical Co. (St. Louis, MO). The substances applied in the first round of screening were mixed (powder), dissolved in ethanol (0.2-0.4 M each), and further diluted with the high  $[K^+]$  perfusing solution to 10-20 mM stock solutions. Mibefradil (30 mM) was dissolved in ethanol, ruthenium red (20 mM) in distilled water, mercuric chloride (30 mM) in high  $[K^+]$  perfusing solution and zinc chloride (30 mM) in 10 mM HCl to prevent the formation of zinc oxychloride precipitate. These stock solutions were diluted further to the desired concentration before the measurements.

### **Cloning of mouse 2PK<sup>+</sup> channels**

Total RNA was isolated from mouse tissues with TRIZOL Reagent (Invitrogen, Paisley, UK) according to the manufacturer's instructions. The RNA was denatured (70°C: 4 min) in the presence of random hexanucleotides (Promega) and reverse transcribed by MMLV-RT (Fermentas) at 37°C: 40 min, followed with 42°C: 20 min. TASK-1, TASK-3 and TWIK-2 coding regions were amplified by the high fidelity Pfu Turbo polymerase (Stratagene); TALK-1

was amplified by HotStar Taq (QIAGEN); TASK-2, THIK-1 and TREK-2 were amplified by 5 cycles with HotStar Taq followed by a 10-fold dilution and 31 cycles with Pfu Turbo. In the TASK-3 Pfu reaction, 2 % DMSO was included for promoting denaturation. Denaturing temperatures for Pfu and HotStar Taq reactions were 98 and 94°C (30-60 sec in the cycles), and the initial denaturations lasted 2 and 14 minutes, respectively. Annealing temperatures, numbers of cycles and primer sequences are given in Table 1 for each reaction. In some cases the touchdown PCR methodology was applied, the annealing temperature was decreased in every 3 cycles at the beginning of the reaction. Extensions were performed at 72°C, for 110-140 sec in the cycles, and there was a 5 min final extension at the end of the reaction.

Taking advantage of the EcoRI and XhoI compatible restriction enzyme sites incorporated into the 5' end of the forward and reverse primers (see Table 1.), respectively, the PCR products were cleaved and cloned between the EcoRI and XhoI sites of pEXO vector. Thus the complete coding sequences of the mouse channels were positioned between the 5' and 3' untranslated regions of the Xenopus globin gene, present in pEXO to increase the stability of the cRNA transcripts in Xenopus oocytes. The fidelity of our clones was verified by automatic sequencing and comparison to published, genomic and EST data. No mutation was generated during the PCR reactions.

### **In vitro site-directed mutagenesis of mouse TRESK**

In vitro site-directed mutagenesis was performed according to the manufacturer's instructions using the QuikChange™ site-directed mutagenesis kit (Stratagene). Complementary primer pairs were designed, coding for the desired mutation together with discriminating silent



mutations (introducing new restriction enzyme sites). The sense primer sequences are listed in Table 2. The mutant clones were identified by restriction enzyme mapping and automatic sequencing.

### **Synthesis of ion channel cRNA**

All channel coding regions (including the newly amplified mouse 2PK<sup>+</sup> channels, our formerly published mTRESK and hTRESK (Czirják *et al.*, 2004) and those kindly provided by others) were cloned or subcloned to pEXO. These DNA templates were linearized at the XbaI site of the vector and purified with QIAGEN PCR Purification Kit. The cRNAs coding for the channels were synthesized in vitro using the Ambion mMESSAGE mMACHINE™ T7 in vitro transcription kit, according to the manufacturer's instructions.

### **Animals and tissue preparation and *Xenopus laevis* oocyte injection**

Oocytes were prepared as previously described (Czirják and Enyedi, 2003). The cells were injected one day after defolliculation. Fifty nanoliters of the appropriate cRNA solution was delivered with Nanoliter Injector (World Precision Instruments, Sarasota, Florida, USA). Electrophysiological experiments were performed three or four days after the injection. All treatments of the animals were conducted in accordance with state laws, institutional regulations and NIH guidelines. The experiments were approved by the Animal Care and Ethics Committee of the Semmelweis University.

## Electrophysiological recordings

Membrane currents of whole oocytes were recorded by two-electrode voltage clamp (OC-725-C Warner Instrument Corporation, Hamden, CT) using microelectrodes made of thin-walled borosilicate glass (Clark Electromedical Instruments, Pangbourne, UK) with resistance of 0.3-1 M $\Omega$  when filled with 3 M KCl. Currents were filtered at 1 kHz and digitally sampled at 1-2.5 kHz. Low [K<sup>+</sup>] solution contained (in mM): NaCl 95.4, KCl 2, CaCl<sub>2</sub> 1.8, HEPES 5 (pH 7.5 with NaOH). High [K<sup>+</sup>] perfusing solution contained 80 mM K<sup>+</sup> (78 mM Na<sup>+</sup> of the low [K<sup>+</sup>] solution was replaced with K<sup>+</sup>). Background K<sup>+</sup> currents were measured in high EC [K<sup>+</sup>] at the end of 300 ms long voltage steps to -100 mV applied in every 3 seconds. The holding potential was 0 mV. For estimating the amplitude of the background current, the inward current in high [K<sup>+</sup>] was corrected for the small nonspecific leak measured in 2 mM EC [K<sup>+</sup>] at -100 mV.

Currents of *Xenopus* outside-out membrane patches were recorded with Axopatch 1D amplifier (Axon Instruments, Foster City, CA) using microelectrodes made of thick-walled borosilicate glass (Clark Electromedical Instruments) with resistance of 30-80 M $\Omega$  when coated with R-6101 elastomer (Dow Corning, Midland, MI), fire-polished and filled with pipette solution, containing (in mM): KCl 140, MgCl<sub>2</sub> 2, EGTA 5, HEPES 10 (pH 7.3 with NaOH). Bath solution contained (in mM): KCl 140, CaCl<sub>2</sub> 1, MgCl<sub>2</sub> 4, HEPES 10 (pH 7.4 with NaOH). Oocytes were devitellinized manually in a hyperosmotic solution, containing (in mM): DL-aspartic acid 200, KCl 20, MgCl<sub>2</sub> 1, EGTA 5, HEPES 10 (pH 7.4 with KOH). For low noise recordings, seal resistance was above 20 G $\Omega$ . Cut-off frequency of the eight-pole Bessel filter was adjusted to 2 kHz, data were acquired at 10 kHz, and the recordings were not filtered further. The charge carrier of the single channel events recorded at -90 mV was verified to be K<sup>+</sup> in all

examined patches by transiently substituting 136 mM  $K^+$  with  $Na^+$  in the bath solution (not shown).

Membrane currents of COS-7 cells were recorded with RK-400 amplifier (Biologic, Claix, France) using microelectrodes made of thin-walled borosilicate glass (Clark Electromedical Instruments) with resistance of 3-9 M $\Omega$  when fire-polished and filled with the same pipette solution as used for single channel recording. Low (4 mM) and high (140 mM)  $[K^+]$  bath solutions also had the same composition as those used for *Xenopus* membrane patches.

All experiments were carried out at room temperature, and solutions were applied by gravity driven perfusion systems. Recordings were digitally sampled by Digidata Interface 1200 (Axon Instruments). Recording and data analysis were performed using pCLAMP software 6.0.4 (Axon Instruments).

### **Statistics and calculations**

Data are expressed as means $\pm$ SEM. Normalized dose-response curves were fitted by least squares method (Origin 6.0, Microcal Software Inc., Northampton, MA) to Hill equation of the form:  $y=1/(1+(c/K_{1/2})^n)$ , where  $c$  is the concentration,  $K_{1/2}$  is the concentration at which half-maximal inhibition occurs and  $n$  is the Hill coefficient. If the inhibition was not complete, a modified form of the Hill equation was used:  $y=\alpha/(1+(c/K_{1/2})^n)+(1-\alpha)$ , where  $\alpha$  is the fraction inhibited by the treatment. Zero segments were detected and the average current of single channel traces was calculated by a computer program developed in our laboratory. Statistical significance was estimated by the nonparametric Mann-Whitney U test, and 1- or 2-way ANOVA followed by Tukey honest significant difference (HSD) test for post hoc pairwise comparisons (Statistica 6.0

MOLPHARM/2005/18556

program package, Statsoft, Tulsa, OK), and the difference was considered to be significant at  $p < 0.05$ .

## RESULTS

### **Mibefradil, zinc and mercuric ions inhibit mouse TRESK, expressed in *Xenopus* oocytes, at micromolar concentration**

The effect of the inhibitors on the inward background  $K^+$  current was measured by the two-electrode voltage clamp technique in high (80 mM) extracellular  $[K^+]$  at -100 mV, in *Xenopus laevis* oocytes expressing mouse TRESK. Inhibitors of mouse TRESK were searched by screening the substances available in our laboratory. In the first round of screening, 24 mixtures, each containing 10 different substances at 5-10 micromolar concentration, were tested. In the second round, constituents of the 3 mixtures, yielding the highest inhibitions in the first round, were examined separately. From these 30 substances, mibefradil, zinc and mercuric ions emerged as the effective agents.

Next, the dose-response relationships of our 3 identified channel blockers were determined. Mibefradil inhibited mouse TRESK with  $IC_{50}$  of 2.2  $\mu$ M (Fig. 1.A and B.), whereas the inhibition by zinc had a slightly higher  $IC_{50}$ , 5.3  $\mu$ M (Fig. 1.D and E.). The effects of mibefradil and zinc were characterized by Hill-coefficients of 0.75 and 0.78, respectively, suggesting that one inhibitor molecule/ion bound to one TRESK channel. For both substances, the inhibition appeared instantaneously and it was readily reversible (Fig. 1.C and F.). In contrast, mercuric ion inhibited mTRESK slowly, and the kinetics of inhibition depended apparently on the concentration of the ion (Fig. 2.A.). The effect of  $Hg^{2+}$  was detectable even at a concentration as low as 100 nM, however, steady-state inhibition by this concentration was not established in 2.5 minutes. Therefore the exact  $IC_{50}$  for  $Hg^{2+}$  has not been determined, but it is apparent in Fig.

2.A., that the value must be smaller than 1  $\mu\text{M}$ . Recovery from mercuric inhibition was very slow (Fig. 2.B.), and thus the inhibition may be regarded irreversible in most applications.

### **Zinc and mercuric ions discriminate TRESK from the other mouse 2PK<sup>+</sup> channels, but mibefradil fails to distinguish it well**

For determining whether a background K<sup>+</sup> current is constituted by TRESK, an inhibitor specific for TRESK within the 2PK<sup>+</sup> channel family is suitable. Therefore the effects of our TRESK inhibitors were examined on the known functional mouse 2PK<sup>+</sup> channels. Mouse TRAAK and TREK-1 were already available in our laboratory. The sequence of mouse TALK-1, TASK-1, TASK-2 and THIK-1 were published and/or deposited to GeneBank (NCBI) previously (BD170722, NM010608, NM021542 and NM\_146037, respectively), and these channels were cloned by RT-PCR from pancreas, cerebellum, kidney and testis RNA, respectively, based on this information. The cloning of TASK-3, TREK-2 and TWIK-2 has not been reported from mouse, thus the sequences of the murine homologs of these channels were determined by comparing the published sequences to the mouse genomic and expressed sequence tag (EST) databases (NCBI GeneBank). The newly derived sequences were also amplified by RT-PCR (TASK-3 and TREK-2 from cerebellum, TWIK-2 from kidney RNA), cloned and expressed in *Xenopus* oocytes. (The new mouse 2PK<sup>+</sup> channel sequences were deposited to GeneBank under the accession numbers: TASK-3 (DQ185133); TREK-2 (DQ185134); TWIK-2 (DQ185135).)

After measuring the effect of mibefradil (3  $\mu\text{M}$ ) on five further 2PK<sup>+</sup> channel types (some members of the TASK and TREK subfamilies, see Fig.3.A) it became clear that the drug inhibited all of them, and the extent of the inhibition was not remarkably different from one

channel to the other. Especially the inhibition of TASK-1 ( $47\pm 2\%$ ) was close to the value characteristic for TRESK ( $60\pm 1\%$ ). Thus mibefradil cannot be applied as a specific TRESK inhibitor within the  $2\text{PK}^+$  channel family.

Mouse TRESK was inhibited more strongly ( $65\pm 3\%$ ) by zinc ( $10\ \mu\text{M}$ ) than the other  $2\text{PK}^+$  channels ( $p < 0.001$ , Tukey HSD test for all mTRESK vs. other channel comparisons, Fig.3.B). Interestingly, human TRESK was not influenced under identical conditions ( $2\pm 2\%$  inhibition), suggesting that the sensitivity to low concentrations of zinc is not a general property of TRESK, but depends on the examined species. Most of the other mouse  $2\text{PK}^+$  channels were slightly activated by  $\text{Zn}^{2+}$  or were not influenced at all. Apart from TRESK, only TASK-3 and TRAAK were inhibited by the ion, however, the inhibition was weak ( $13\pm 2\%$  and  $11\pm 2\%$ , respectively). As it has been reported (Czirják and Enyedi, 2002) that both TASK-3 and TRAAK are sensitive to ruthenium red (RR), we also examined the effect of  $\text{Zn}^{2+}$  on TRESK in the presence of RR. High ( $10\ \mu\text{M}$ ) concentration of RR induced maximal block of TASK-3 and TRAAK, but caused only negligible TRESK inhibition ( $15\pm 2\%$ , Fig. 4. A., B., C.). In the presence of RR, zinc failed to inhibit TASK-3 and TRAAK further (1 % inhibition and 2 % activation, respectively, expressed in the percent of the original current), but the extent of the additional TRESK inhibition (55 %) induced by the administration of zinc in the presence of RR was similar to that measured in the absence of RR (Fig. 4. D). Thus zinc is even more selective for TRESK in the presence of ruthenium red. Sensitivity to zinc, after the elimination of TASK-3 and TRAAK currents by ruthenium red, is a distinctive feature of TRESK among the mouse  $2\text{PK}^+$  channels.

TRESK was by far the most strongly inhibited  $2\text{PK}^+$  channel by mercuric ion ( $72\pm 4$  and  $78\pm 2\%$  inhibition for the human and mouse channel, respectively, by  $3\ \mu\text{M}\ \text{Hg}^{2+}$ ,  $p < 0.03$ , Tukey

HSD test for all mTRESK or hTRESK vs. other channel comparisons, see Fig.3.C). THIK-1 was the only other inhibited  $2\text{PK}^+$  channel, however, its inhibition was much weaker ( $13\pm 2\%$ ) than that of TRESK. Some members of the TASK and TREK subfamilies (TASK-3, TREK-1 and TREK-2) were activated by more than 50% by  $3\ \mu\text{M}\ \text{Hg}^{2+}$ . This activation may mask TRESK inhibition, if one of these channels was coexpressed with TRESK in comparable quantity. However, the pattern of mercuric inhibition of mouse  $2\text{PK}^+$  channels unequivocally suggests that the strong reduction of a background  $\text{K}^+$  current of unknown composition by mercuric ion is a predicting indicator of the significant contribution of TRESK to that examined current.

### **Inhibition of mouse TRESK by zinc and mercuric ions in mammalian COS-7 cells is voltage-independent**

Cytosolic and membrane composition of the oocyte of amphibian *Xenopus laevis* may differ in many aspects from those of mammalian cells. To exclude the possibility that the mechanism of action of our inhibitors relied on oocyte specific components, we also expressed mouse TRESK in the mammalian COS-7 cell line, and measured its sensitivity to  $\text{Zn}^{2+}$  and  $\text{Hg}^{2+}$  with the whole cell patch clamp technique. In this experiment the degree of voltage-dependence of the inhibition was estimated by a slow ramp protocol in identical 140 mM extra- and intracellular  $[\text{K}^+]$ . Under these conditions, the background TRESK current was a nearly linear function of the voltage with a reversal potential at 0 mV (Fig. 5.). Application of both  $\text{Zn}^{2+}$  and  $\text{Hg}^{2+}$  simply transformed this current-voltage relationship to a less steep line, indicating that the inhibition was not voltage-dependent (Fig.5.B and D). The extent of inhibition ( $51\pm 4\%$  for  $\text{Zn}^{2+}$  ( $10\ \mu\text{M}$ ,  $n=5$ ) and  $88\pm 1\%$  for  $\text{Hg}^{2+}$  ( $3\ \mu\text{M}$ ,  $n=5$ )) was similar to that obtained in *Xenopus* oocytes.



### **Zinc and mercuric ions inhibit TRESK also at the single channel level in excised, outside-out membrane patches**

To prove that the effect of  $\text{Hg}^{2+}$  and  $\text{Zn}^{2+}$  is membrane-delimited, and does not depend on an intracellular indirect mechanism, the inhibitors were also tested in a cell-free system, outside-out membrane patches of *Xenopus* oocytes. These patches contained only a few mTRESK channels, and the composition of the solution on both sides of the membrane was controlled experimentally, excluding the possibility of the interaction of cytosolic regulators. The inward current of a single active mTRESK channel at -90 mV in symmetrical 140 mM  $[\text{K}^+]$  is characterized by trains of short (typically <2 ms) spike-like openings (see inset in Fig. 6), and consequently the flickery currents of a few channels are summed up to an irregular control curve of higher amplitude (Fig. 6. A. and C., *upper* curves). Because this type of activity does not allow the estimation of the probability of opening and unitary current separately, instead of these parameters we calculated the average current from the curves. Both  $\text{Hg}^{2+}$  (3  $\mu\text{M}$ ) and  $\text{Zn}^{2+}$  (30  $\mu\text{M}$ ) reduced the average single channel current (see Fig. 6. A. and C for representative traces, and Fig. 6. B. and D. for statistical analysis). This indicates that the action of  $\text{Hg}^{2+}$  and  $\text{Zn}^{2+}$  is membrane-delimited, and the most probable target of the ions is TRESK channel itself.

### **Mutation of extracellular cysteine residues at position 77 and 82 to serines significantly decreases the inhibition by mercuric ion**

As  $\text{Hg}^{2+}$  inhibits many target proteins by binding to the SH groups of cysteine residues,

we mutated all extracellular cysteines of mouse TRESK to serines one by one, or in pairs, where the residues were close to each other. Some of these mutations reduced severely the  $K^+$  current obtained by expressing the channel in *Xenopus* oocytes. When cysteine 329 was mutated to serine in the second EC loop, no  $K^+$  current could be measured. TRESK C77,82S double mutant produced  $0.6 \pm 0.1 \mu A$  ( $n=6$ ) background  $K^+$  current, when its cRNA was microinjected at 25-fold higher concentration than that of the wild type (inducing  $2.6 \pm 0.3 \mu A$  in the same oocyte preparation,  $n=7$ ). Nevertheless, the expression of C121,122S, C77,82S and C95S mutants (first EC loop) allowed the measurement of their  $Hg^{2+}$  sensitivity (Fig. 7). While the sensitivity of the C121,122S and C95S mutants was not significantly different from the wild type, the C77,82S mutant was much less inhibited ( $43 \pm 6\%$  inhibition) than the wild type ( $76 \pm 3\%$  inhibition). Therefore cysteine 77 and 82 may contribute to the  $Hg^{2+}$  binding site of mouse TRESK.

**H132Y,M133I double mutation decreases mTRESK sensitivity to zinc, while Y121H,I122M double mutation of hTRESK enhances the inhibition by the ion**

Zinc was suggested to interact with histidine 98 residue located directly after the GYG  $K^+$  channel signature sequence in the first pore domain of TASK-3 (Clarke *et al.*, 2004). Since mouse TRESK contains histidine after its GYG, but human TRESK has a tyrosine, it was feasible to assume that this may contribute to the different zinc sensitivity of mouse and human TRESK channels. It has been recently reported that mutating the histidine to tyrosine in mTRESK or mutating the tyrosine to histidine in hTRESK resulted in nonfunctional subunits (Keshavaprasad *et al.*, 2005). Because the pore domain sequence of mTRESK (FSTVGYGHMYPVTRL) differs from that of hTRESK (FSTVGYGYIYPVTRL) only in two amino acids in this region, we

MOLPHARM/2005/18556

hypothesised that both residues have to be interchanged to obtain functional channels. Indeed, both the mTRESK double mutant containing YI instead of HM and the hTRESK double mutant containing HM instead of YI were functional in *Xenopus* oocytes. Inhibition of the double mutant mTRESK by  $Zn^{2+}$  was deteriorated (IC50 increased to 157  $\mu$ M from 5.3  $\mu$ M characteristic for the wild type, Fig. 8.A), whereas the double mutant hTRESK became slightly sensitive to  $Zn^{2+}$  (Fig. 8.B). The remaining inhibition of the double mutant mTRESK and the limited efficacy and potency of  $Zn^{2+}$  toward the double mutant human channel suggest that other residues may also be involved in the constitution of the zinc binding site, however, our results clearly indicate that the pore vicinal histidine plays a pivotal role in the determination of zinc sensitivity.

## DISCUSSION

Mibefradil, zinc and mercuric ions have been applied extensively in the investigation of ion channel functions. Mibefradil was originally described as a selective inhibitor of the low voltage-activated (LVA), T-type calcium channels (Mishra and Hermsmeyer, 1994). A wide range of IC<sub>50</sub> values (around 0.1-3  $\mu$ M) was reported in different studies, since the potency of mibefradil for T channels was highly dependent on the examined preparations, and even in the case of cloned calcium channels, it was strongly influenced by the experimental conditions (Martin *et al.*, 2000). In certain cell types, the drug was not selective enough to distinguish between T- and the high voltage-activated (HVA), L-type calcium channels, and potassium conductances were also modified by the same (or even lower) drug concentration (Liu *et al.*, 1999).

Mainly, the delayed and inward rectifier K<sup>+</sup> channels were highly sensitive to mibefradil (Chouabe *et al.*, 1998; Gomora *et al.*, 1999; Perchenet and Clement-Chomienne, 2000). Recently, it has also been described, that mibefradil inhibited the background K<sup>+</sup> current of bovine adrenal zona fasciculata cells, and its equivalent 2PK<sup>+</sup> channel, bovine TREK-1 expressed in HEK-293 cells, with IC<sub>50</sub> of 0.5  $\mu$ M (Enyeart *et al.*, 2002). In our experiment, mouse TREK-1 was less sensitive to the drug (23 % inhibition by 3  $\mu$ M). This may reflect species difference, however, the amino acid sequences of bovine and mouse TREK-1 are 97 % identical. Alternatively, TREK-1 inhibition by mibefradil may be strongly dependent on the experimental conditions, similarly to the case of T-type calcium channel.

Mibefradil was identified as a potent inhibitor of mouse TRESK by our screening procedure. Although TRESK was blocked most potently, mibefradil inhibited all 2PK<sup>+</sup> channels examined in this study, and the slight differences of the inhibitions indicated that mibefradil

cannot be used as a selective TRESK inhibitor. Therefore, in addition to delayed and inward rectifiers, mibefradil is a non-specific inhibitor of  $2\text{PK}^+$  channels too. Our results reinforce the view that besides T-type voltage-gated calcium channels modification of several potassium conductances (including those of  $2\text{PK}^+$  channels) may have contributed to the side effects of this drug, formerly used as an antihypertensive medicine.

Whereas mercuric ion is an insidious environmental pollutant, zinc is an important trace element, essential for life, and incorporated in the active site of many enzymes. Accordingly, zinc-specific transporters have evolved, and the distribution of  $\text{Zn}^{2+}$  is regulated by these proteins (Liuzzi and Cousins, 2004). One example for zinc compartmentalization is the sequestration of the ion in zinc-containing neurons (Takeda, 2000). In response to depolarization, zinc is released from the synaptic vesicles of these specialized glutamatergic neurons and its concentration is estimated to reach levels between 10-100  $\mu\text{M}$  in the synaptic cleft (Vogt *et al.*, 2000; Li *et al.*, 2001). This concentration may modulate several ion conductances, and it has been recently suggested, that some  $2\text{PK}^+$  channels are also possible targets of the synaptically released zinc. Human TASK-3 was inhibited by zinc with  $\text{IC}_{50}$  values of 12.7 and 19.8  $\mu\text{M}$  in HEK-293 cells and *Xenopus* oocytes, respectively (Gruss *et al.*, 2004; Clarke *et al.*, 2004). In turn, TREK-2 was activated by zinc in *Xenopus* oocytes with  $\text{EC}_{50}$  of 87.1  $\mu\text{M}$ , and this activation was suggested to be a specific hallmark of TREK-2 among the  $2\text{PK}^+$  channels (Kim *et al.*, 2005).

In this study, we performed the systematic analysis of zinc sensitivity of functional mouse  $2\text{PK}^+$  channels. From the 15 cloned mammalian  $2\text{PK}^+$  channel subunits, 12 form functional plasma membrane channels in *Xenopus* oocytes. It has been reported that KCNK7 (a member of the TWIK family, (Salinas *et al.*, 1999)), TASK-5 (Kim and Gnatenco, 2001) and THIK-2 (Rajan *et al.*, 2001) cannot be functionally expressed. Although in some studies small TWIK-1 and

TWIK-2 currents were measured after high overexpression (Lesage *et al.*, 1996; Chavez *et al.*, 1999), it has been recently described that a specific mechanism targets the vast majority of TWIK-1 channels to recycling endosomes (Decressac *et al.*, 2004). Therefore the dominant location of members of the TWIK family may be intracellular. Similarly to previous observations (Goldstein *et al.*, 1998; Pountney *et al.*, 1999), we did not obtain currents by expressing the original mouse TWIK-1 (Lesage *et al.*, 1997) or our sequence verified mouse TWIK-2 clone in *Xenopus* oocytes. Mouse TALK-2 has not been cloned, since its genomic sequence was incomplete in GeneBank. Zinc sensitivity of the remaining nine functional mouse 2PK<sup>+</sup> channels were tested.

Our results are in accordance with the published data in the sense that TASK-3 was slightly inhibited, and TREK-2 was slightly activated by 10  $\mu\text{M}$  Zn<sup>2+</sup>. However, TREK-1 was also activated identically in *Xenopus* oocytes, indicating that the two closely related TREK channels share the property of activation by zinc. Thus our data do not support the conclusion of Kim *et al.* that activation by zinc is specific for TREK-2 among the 2PK<sup>+</sup> channels. Furthermore, considering the zinc resistance of human TREK-1 in HEK-293 cells (Gruss *et al.*, 2004), it seems that the activation of TREK-1 by Zn<sup>2+</sup> depends on the examined species or the applied expression system.

Zinc inhibited mouse TRESK with IC<sub>50</sub> values of 5.3 and 10  $\mu\text{M}$  in *Xenopus* oocytes and in COS-7 cells, respectively. Although these values are smaller than those published previously for any of the 2PK<sup>+</sup> channels, they are close to the IC<sub>50</sub> of TASK-3. Moreover, in addition to TRESK and TASK-3, we detected slight inhibition of one further 2PK<sup>+</sup> channel, TRAAK, by zinc. These results indicate that, by using zinc alone, these 3 channel types cannot be discriminated efficiently. However, as a lucky coincidence, TASK-3 and TRAAK channels were

reported to be highly sensitive to ruthenium red (Czirják and Enyedi, 2002). We also demonstrated formerly that glutamate 70 residues of both TASK-3 subunits of the homodimer were required for the binding of a single RR molecule (Czirják and Enyedi, 2003). Later, the importance of the same TASK-3 residues in the binding of zinc was emphasized (Clarke *et al.*, 2004). The inhibitory mechanism of TRAAK is different from that of TASK-3, since the effect of RR on TRAAK is characterized by a Hill-coefficient of 2.1 (Czirják and Enyedi, 2002), suggesting the involvement of multiple (most probably two) binding sites on TRAAK homodimer. Presently it is unknown, whether RR and  $Zn^{2+}$  interact with the same amino acid side chains in TRAAK. Whereas TASK-3 and TRAAK were blocked by both RR and  $Zn^{2+}$ , TRESK was only negligibly influenced by high concentrations of RR. Therefore the zinc binding site of TRESK does not bind RR, and consequently, inhibition by zinc in the presence of ruthenium red is diagnostic for TRESK among the  $2PK^+$  channels.

Mercuric ion has been used as an inhibitor of water channels, aquaporins (Gunnarson *et al.*, 2004).  $Hg^{2+}$  inhibits aquaporins by binding to certain cysteine residues (Preston *et al.*, 1993), and as a SH-reagent, it also modifies dozens of other enzymatic reactions and transport mechanisms. To our knowledge, the effect of  $Hg^{2+}$  on  $2PK^+$  channels has not been investigated so far. Herein we report that mercuric ion is a potent inhibitor of both mouse and human TRESK, while it activates mouse TASK-3, TREK-1 and TREK-2 markedly. Localization of the  $Zn^{2+}$  and  $Hg^{2+}$  binding sites on the external face of TRESK was strongly supported by the effect of the ions in outside-out membrane patches. The voltage-independent inhibition by these inorganic blockers indicated that the sites of interaction are outside the transmembrane electrical field. The pore vicinal histidine 132 was identified as a major contributor to the zinc binding site of mouse TRESK. This is similar to the voltage-independent inhibition of TASK-3 by  $Zn^{2+}$ , where histidine

98 was reported to be involved in the inhibitory mechanism in addition to glutamate 70 (Clarke *et al.*, 2004). The slowly developing and practically irreversible inhibition by  $\text{Hg}^{2+}$  suggested that this ion acted as a SH-reagent. Replacing each extracellular cysteine with serine (its closest structural analogue) resulted in two mutant channels, significantly different from the wild type. While the C329S mutant was not functional, the C77,82S double mutant expressed a smaller current, which was less sensitive to  $\text{Hg}^{2+}$ . Accordingly, these residues are likely constituents of the  $\text{Hg}^{2+}$  binding site.

High sensitivity of TRESK, TASK-3, TREK-1 and TREK-2 to  $\text{Hg}^{2+}$  and their expression in the central nervous system suggest that the modulation of these  $2\text{PK}^+$  channels may contribute to the ataxia, visual and auditory deficits and other neurotoxic effects of mercuric ion. While  $\text{Hg}^{2+}$  may bind to  $2\text{PK}^+$  channels in vivo only in the case of poisoning, binding of zinc may also happen physiologically, as it was suggested for TASK-3 previously (Gruss *et al.*, 2004; Clarke *et al.*, 2004). Nevertheless, it is intriguing that the zinc sensitivity of TRESK does not seem to be evolutionary conserved, or at any rate, there is tremendous difference in the affinities between mice and humans. Whether we will learn in the future that zinc regulates TRESK physiologically, or not, it can be stated unambiguously that zinc and mercuric ions are valuable pharmacological tools for the identification of TRESK in electrophysiological experiments.



## Acknowledgments

The authors thank Professor M. Lazdunski and Dr. F. Lesage for pEXO, pEXO-mTRAAK, pEXO-mTREK-1 and pBS-mTWIK plasmids. The expert technical assistance of Mrs. Irén Veres and Mrs. Beáta Busi is highly appreciated.

## References

Bayliss DA, Sirois JE and Talley EM (2003) The TASK Family: Two-Pore Domain Background K<sup>+</sup> Channels. *Mol Interv* **3**:205-219.

Berg AP, Talley EM, Manger JP and Bayliss DA (2004) Motoneurons Express Heteromeric TWIK-Related Acid-Sensitive K<sup>+</sup> (TASK) Channels Containing TASK-1 (KCNK3) and TASK-3 (KCNK9) Subunits. *J Neurosci* **24**:6693-6702.

Chavez RA, Gray AT, Zhao BB, Kindler CH, Mazurek MJ, Mehta Y, Forsayeth JR and Yost CS (1999) TWIK-2, a New Weak Inward Rectifying Member of the Tandem Pore Domain Potassium Channel Family. *J Biol Chem* **274**:7887-7892.

Chouabe C, Drici MD, Romey G, Barhanin J and Lazdunski M (1998) HERG and KvLQT1/IsK, the Cardiac K<sup>+</sup> Channels Involved in Long QT Syndromes, Are Targets for Calcium Channel Blockers. *Mol Pharmacol* **54**:695-703.

Clarke CE, Veale EL, Green PJ, Meadows HJ and Mathie A (2004) Selective Block of the Human 2-P Domain Potassium Channel, TASK-3, and the Native Leak Potassium Current, IKSO, by Zinc. *J Physiol* **560**:51-62.

Czirják G and Enyedi P (2002) Formation of Functional Heterodimers Between the TASK-1 and TASK-3 Two-Pore Domain Potassium Channel Subunits. *J Biol Chem* **277**:5426-5432.

Czirják G and Enyedi P (2003) Ruthenium Red Inhibits TASK-3 Potassium Channel by Interconnecting Glutamate 70 of the Two Subunits. *Mol Pharmacol* **63**:646-652.

Czirják G, Tóth ZE and Enyedi P (2004) The Two-Pore Domain K<sup>+</sup> Channel, TRESK, Is Activated by the Cytoplasmic Calcium Signal Through Calcineurin. *J Biol Chem* **279**:18550-18558.

Decressac S, Franco M, Bendahhou S, Warth R, Knauer S, Barhanin J, Lazdunski M and Lesage F (2004) ARF6-Dependent Interaction of the TWIK1 K<sup>+</sup> Channel With EFA6, a GDP/GTP Exchange Factor for ARF6. *EMBO Rep* **5**:1171-1175.

Enyeart JJ, Xu L, Danthi S and Enyeart JA (2002) An ACTH- and ATP-Regulated Background K<sup>+</sup> Channel in Adrenocortical Cells Is TREK-1. *J Biol Chem* **277**:49186-49199.

Goldstein SA, Bockenhauer D, O'Kelly I and Zilberberg N (2001) Potassium Leak Channels and the KCNK Family of Two-P-Domain Subunits. *Nat Rev Neurosci* **2**:175-184.

Goldstein SA, Wang KW, Ilan N and Pausch MH (1998) Sequence and Function of the Two P Domain Potassium Channels: Implications of an Emerging Superfamily. *J Mol Med* **76**:13-20.

Gomora JC, Enyeart JA and Enyeart JJ (1999) Mibefradil Potently Blocks ATP-Activated K<sup>+</sup> Channels in Adrenal Cells. *Mol Pharmacol* **56**:1192-1197.

Gruss M, Mathie A, Lieb WR and Franks NP (2004) The Two-Pore-Domain K<sup>+</sup> Channels TREK-

1 and TASK-3 Are Differentially Modulated by Copper and Zinc. *Mol Pharmacol* **66**:530-537.

Gunnarson E, Zelenina M and Aperia A (2004) Regulation of Brain Aquaporins. *Neuroscience* **129**:947-955.

Kang D, Han J, Talley EM, Bayliss DA and Kim D (2004a) Functional Expression of TASK-1/TASK-3 Heteromers in Cerebellar Granule Cells. *J Physiol* **554**:64-77.

Kang D, Mariash E and Kim D (2004b) Functional Expression of TRESK-2, a New Member of the Tandem-Pore K<sup>+</sup> Channel Family. *J Biol Chem* **279**:28063-28070.

Keshavaprasad B, Liu C, Au JD, Kindler CH, Cotten JF, Yost CS (2005) Species-specific differences in response to anesthetics and other modulators by the K2P channel TRESK. *Anesth Analg* **101**:1042-9

Kim D and Gnatenco C (2001) TASK-5, a New Member of the Tandem-Pore K<sup>+</sup> Channel Family. *Biochem Biophys Res Commun* **284**:923-930.

Kim JS, Park JY, Kang HW, Lee EJ, Bang H and Lee JH (2005) Zinc Activates TREK-2 Potassium Channel Activity. *J Pharmacol Exp Ther* **314**:618-625.

Larkman PM and Perkins EM (2005) A TASK-Like PH- and Amine-Sensitive 'Leak' K<sup>+</sup> Conductance Regulates Neonatal Rat Facial Motoneuron Excitability in Vitro. *Eur J Neurosci* **21**:679-691.

Lauritzen I, Zanzouri M, Honore E, Duprat F, Ehrenguber MU, Lazdunski M and Patel AJ (2003) K<sup>+</sup>-Dependent Cerebellar Granule Neuron Apoptosis. Role of Task Leak K<sup>+</sup> Channels. *J Biol Chem* **278**:32068-32076.

Lesage F, Guillemare E, Fink M, Duprat F, Lazdunski M, Romey G and Barhanin J (1996) TWIK-1, a Ubiquitous Human Weakly Inward Rectifying K<sup>+</sup> Channel With a Novel Structure. *EMBO J* **15**:1004-1011.

Lesage F, Lauritzen I, Duprat F, Reyes R, Fink M, Heurteaux C and Lazdunski M (1997) The Structure, Function and Distribution of the Mouse TWIK-1 K<sup>+</sup> Channel. *FEBS Lett* **402**:28-32.

Li Y, Hough CJ, Suh SW, Sarvey JM and Frederickson CJ (2001) Rapid Translocation of Zn<sup>2+</sup> From Presynaptic Terminals into Postsynaptic Hippocampal Neurons After Physiological Stimulation. *J Neurophysiol* **86**:2597-2604.

Liu C, Au JD, Zou HL, Cotten JF and Yost CS (2004) Potent Activation of the Human Tandem Pore Domain K<sup>+</sup> Channel TRESK With Clinical Concentrations of Volatile Anesthetics. *Anesth Analg* **99**:1715-22.

Liu JH, Bijlenga P, Occhiodoro T, Fischer-Lougheed J, Bader CR and Bernheim L (1999) Mibefradil (Ro 40-5967) Inhibits Several Ca<sup>2+</sup> and K<sup>+</sup> Currents in Human Fusion-Competent Myoblasts. *Br J Pharmacol* **126**:245-250.

Liuzzi JP and Cousins RJ (2004) Mammalian Zinc Transporters. *Annu Rev Nutr* **24**:151-172.

MOLPHARM/2005/18556

Maingret F, Lauritzen I, Patel AJ, Heurteaux C, Reyes R, Lesage F, Lazdunski M and Honore E (2000) TREK-1 Is a Heat-Activated Background K<sup>+</sup> Channel. *EMBO J* **19**:2483-2491.

Martin RL, Lee JH, Cribbs LL, Perez-Reyes E and Hanck DA (2000) Mibefradil Block of Cloned T-Type Calcium Channels. *J Pharmacol Exp Ther* **295**:302-308.

Mishra SK and Hermsmeyer K (1994) Selective Inhibition of T-Type Ca<sup>2+</sup> Channels by Ro 40-5967. *Circ Res* **75**:144-148.

Perchenet L and Clement-Chomienne O (2000) Characterization of Mibefradil Block of the Human Heart Delayed Rectifier HKv1.5. *J Pharmacol Exp Ther* **295**:771-778.

Pountney DJ, Gulkarov I, Vega-Saenz de ME, Holmes D, Saganich M, Rudy B, Artman M and Coetzee WA (1999) Identification and Cloning of TWIK-Originated Similarity Sequence (TOSS): a Novel Human 2-Pore K<sup>+</sup> Channel Principal Subunit. *FEBS Lett* **450**:191-196.

Preston GM, Jung JS, Guggino WB and Agre P (1993) The Mercury-Sensitive Residue at Cysteine 189 in the CHIP28 Water Channel. *J Biol Chem* **268**:17-20.

Rajan S, Wischmeyer E, Karschin C, Preisig-Muller R, Grzeschik KH, Daut J, Karschin A and Derst C (2001) THIK-1 and THIK-2, a Novel Subfamily of Tandem Pore Domain K<sup>+</sup> Channels. *J Biol Chem* **276**:7302-7311.

Salinas M, Reyes R, Lesage F, Fosset M, Heurteaux C, Romey G and Lazdunski M (1999)

MOLPHARM/2005/18556

Cloning of a New Mouse Two-P Domain Channel Subunit and a Human Homologue With a Unique Pore Structure. *J Biol Chem* **274**:11751-11760.

Sano Y, Inamura K, Miyake A, Mochizuki S, Kitada C, Yokoi H, Nozawa K, Okada H, Matsushime H and Furuichi K (2003) A Novel Two-Pore Domain K<sup>+</sup> Channel, TRESK, Is Localized in the Spinal Cord. *J Biol Chem* **278**:27406-27412.

Takeda A (2000) Movement of Zinc and Its Functional Significance in the Brain. *Brain Res Brain Res Rev* **34**:137-148.

Talley EM, Lei Q, Sirois JE and Bayliss DA (2000) TASK-1, a Two-Pore Domain K<sup>+</sup> Channel, Is Modulated by Multiple Neurotransmitters in Motoneurons. *Neuron* **25**:399-410.

Vogt K, Mellor J, Tong G and Nicoll R (2000) The Actions of Synaptically Released Zinc at Hippocampal Mossy Fiber Synapses. *Neuron* **26**:187-196.

## Footnotes

This work was supported by the Hungarian National Research Fund (OTKA T46954) and the Hungarian Medical Research Council (ETT-085/2003). Gábor Czirják was supported by the János Bolyai fellowship of the Hungarian Academy of Sciences.

Péter Enyedi, MD, PhD, Department of Physiology, Semmelweis University, P.O.Box 259, Budapest, Hungary, H-1444, Phone: (36-1-) 266-2755/4079; Fax: (36-1-) 266-6504, E-mail: enyedi@puskin.sote.hu



## Legend to Figures

### Fig. 1. Concentration-dependent inhibition of mouse TRESK by mibefradil and zinc.

**A. and D.** Representative currents of *Xenopus* oocytes expressing mTRESK are shown in extracellular solutions of different  $K^+$  and mibefradil (A) or zinc (D) concentrations (as indicated above the curves). The plotted inward currents were measured at the end of 300 ms long voltage steps to -100 mV applied in every 3 s from a holding potential of 0 mV. **B. and E.** Mibefradil (B) and zinc (E) dose-response relationships. Inhibition was measured as shown in panel A and D. The currents were corrected for the small nonspecific leak in 2 mM extracellular  $[K^+]$  at -100 mV and normalized to the value without the inhibitors. Each data point represents the average of normalized currents of 5-7 oocytes. Error bars are smaller than symbols in most cases. The data points were fitted by Hill equation (see methods). **C. and F.** Representative recordings demonstrating reversibility of the inhibition by mibefradil (C) and zinc (F). The method of measurement was the same as in panels A and D.

### Fig. 2. Concentration- and time-dependent inhibition of mouse TRESK by mercuric ion.

**A.** TRESK current expressed in *Xenopus* oocytes was inhibited by different concentrations of mercuric ion, as indicated on the right side. The current was measured in 80 mM EC  $[K^+]$  at -100 mV. Each trace represents the average current of 5 oocytes, normalized to the value before the application of  $Hg^{2+}$ . **B.** Slow recovery of mTRESK current was evoked by extensive washout after a brief exposure to  $Hg^{2+}$  (10  $\mu$ M). Note the long time scale of the recording.

**Fig. 3. Sensitivity of 2PK<sup>+</sup> channels to mibefradil, zinc and mercuric ions.**

Mouse 2PK<sup>+</sup> channels and human TRESK were expressed in *Xenopus* oocytes and their sensitivity to the given inhibitor (shown above the columns) was measured and calculated as in Fig. 1. The numbers in the columns indicate the number of the examined oocytes. Data for mTRESK are repeated from Figures 1 and 2.

**Fig. 4. Among the zinc sensitive mouse 2PK<sup>+</sup> channels, TRESK is the only one being resistant to ruthenium red.**

**A., B. and C.** Representative currents of 3 oocytes expressing mTRESK, mTRAAK and mTASK-3, respectively, were measured with the same voltage protocol as in Fig. 1.A. In 80 mM EC [K<sup>+</sup>], the currents were inhibited first by ruthenium red (10 μM), and subsequently by zinc in the continued presence of ruthenium red (10 μM for both inhibitors), as indicated by the horizontal bars above the curves. At the end of the measurements the small nonspecific leak was estimated by changing the EC [K<sup>+</sup>] to 2 mM. **D.** The currents, inhibited to steady state by ruthenium red (*light columns*) or ruthenium red plus zinc (*dark columns*), were normalized to the current measured before the addition of the inhibitors. For each channel, the average of 4-5 oocytes was depicted.

**Fig. 5. Zinc and mercuric ions inhibit mouse TRESK voltage-independently in COS-7 cells.**

**A. and C.** Representative currents of COS-7 cells expressing TRESK are shown during the application of zinc (A) or mercuric ions (C), as the horizontal bars indicate above the curves. The plotted values were sampled at the end of the voltage steps to -100 mV applied in every 2 s (see the inset between panel B and D for the voltage protocol). The EC 140 mM [K<sup>+</sup>] was reduced

occasionally to 4 mM (as indicated above the curves) for estimating TRESK  $K^+$  current. **B. and D.** Current traces evoked by the voltage ramp protocol in the absence (*gray*) and in the presence of the inhibitor (*black*) were plotted. These current traces correspond to the episodes marked with gray and black vertical arrows in panel A and C.

**Fig. 6. Zinc and mercuric ions reduce TRESK single channel current in outside-out membrane patches of *Xenopus* oocytes.**

**A. and C.** Mouse TRESK single channel activity was detected at -90 mV in symmetrical 140 mM EC and IC  $[K^+]$ , in the absence (*upper curve*) and in the presence (*lower curve*) of  $Zn^{2+}$  (A) or  $Hg^{2+}$  (C). Note the reduced area between the curve and the zero level, and the higher proportion of zero segments in the presence of the inhibitors. Zero current levels are indicated by horizontal arrows. The scale bars in panel C apply to both panels. In the framed inset, representing the TRESK single channel event marked with a vertical arrow, only the time scale was extended. **B. and D.** Every data point in these plots represents the average of a 950 ms long current trace (similar to those illustrated in panel A and C). These current traces were recorded in every 4 s before and after the addition of the inhibitors. The inhibitors were administered at 0 s as indicated by the horizontal black bars. All data points were normalized to the average of the data points measured before the addition of the inhibitor in the same membrane patch. (Thus the values of the control period scatter around 1.) The thick gray curves are constituted by straight lines connecting the moving averages of every 7 ( $Zn^{2+}$ ) or 21 ( $Hg^{2+}$ ) neighboring data points. Data points around 0 s were omitted because of the solution-changing artifact. Both ions inhibited mTRESK significantly ( $p < 10^{-6}$ , Mann-Whitney U-test; in the case of  $Hg^{2+}$  the data points measured after 150 s were compared to those of the control period).

**Fig. 7. Mutation of cysteine 77 and 82 of mouse TRESK to serines reduces mercuric inhibition.**

Wild type and mutant mTRESK channels, in which different extracellular cysteines were replaced by serines, were expressed in *Xenopus* oocytes and their sensitivity to  $\text{Hg}^{2+}$  (10  $\mu\text{M}$ ) was measured as in Fig. 1. The numbers in the columns indicate the number of the examined oocytes. Inhibition of the C77,82S double mutant was significantly weaker than that of the wild type channel ( $p < 0.001$ , Tukey HSD post hoc comparison after 1-way ANOVA).

**Fig. 8. Double mutation of His-Met located directly after the GYG  $\text{K}^+$  channel signature sequence in the first pore domain to Tyr-Ile reduces the  $\text{Zn}^{2+}$  sensitivity of mouse TRESK, whereas double mutation of Tyr-Ile to His-Met in the corresponding position of the human channel engenders  $\text{Zn}^{2+}$  sensitivity.**

**A.** Zinc dose-response relationship of H132Y,M133I double mutant mTRESK (*black*) was measured as in Fig. 1. For comparison, the dose-response relationship of the wild type (wt.) mouse channel (*gray*) was repeated from Fig. 1.E. **B.** Zinc dose-response relationships of the wild type (wt., *gray*) and Y121H,I122M double mutant (*black*) hTRESK channels were plotted. Data points represent the average of normalized currents of 5-9 oocytes, and the error bars are smaller than symbols in most cases. The data points were fitted by Hill equation (panel A) or a modified Hill equation (see methods) for incomplete inhibition (panel B). Dose-response relationships of the wild type and mutant channels were significantly different for both human and mouse TRESK ( $p < 10^{-6}$ , 2-way ANOVA).

Channel	Oligonucleotide (5' → 3')	°C : cycles	Restr. enzyme
mTALK-1	CAGgaattcGCCACCATGCCCGTGCTGGGGTCTG	55:36	EcoRI- XhoI
	GCGctcgagTCATGCAGAGATGGGGATTTTC		
mTASK-1	CAGgaattcGGAGGGACGATGAAGCGGCAG	72:3, 69:3, 66:3, 62:27	EcoRI- XhoI
	GGTGctcgagGTCTGGCTGTGGTTC		
mTASK-2	GCGcaattgTCCAGAGTCATGGTGGACCG	55:36	MunI- XhoI
	GCGctcgagTCACGTGCCCTGGGGTTATC		
mTASK-3	CAGgaattcGCGGCCATGAAGCGGCAG	65:3, 62:3, 59:3, 57:27	EcoRI- Sall
	ATACCgtcgacTTAGATGGACTTGCGACGGAG		
mTHIK-1	CAGgaattcTCCAGTGCCATGGCTGGCCG	55:36	EcoRI- XhoI
	GCGctcgagGTTCTACCTATCTCCACTGGTC		
mTREK-2	GCGcaattgATCCCCCTGTGGGCAACGGAG	55:36	MunI- Sall
	ATACCgtcgacTTTAAGGCACGTGTCTCAGTGTG		
mTWIK-2	CAGgaattcACGGGCACCATGCGGCGGGG	72:3, 69:3, 66:3, 62:27	EcoRI- XhoI
	GCGctcgagGTCGACAGCTACCTGGGGATG		

**Tabl. 1. Oligonucleotide sequences, annealing temperatures and restriction enzyme sites for PCR and cloning of mouse 2PK<sup>+</sup> channels.**

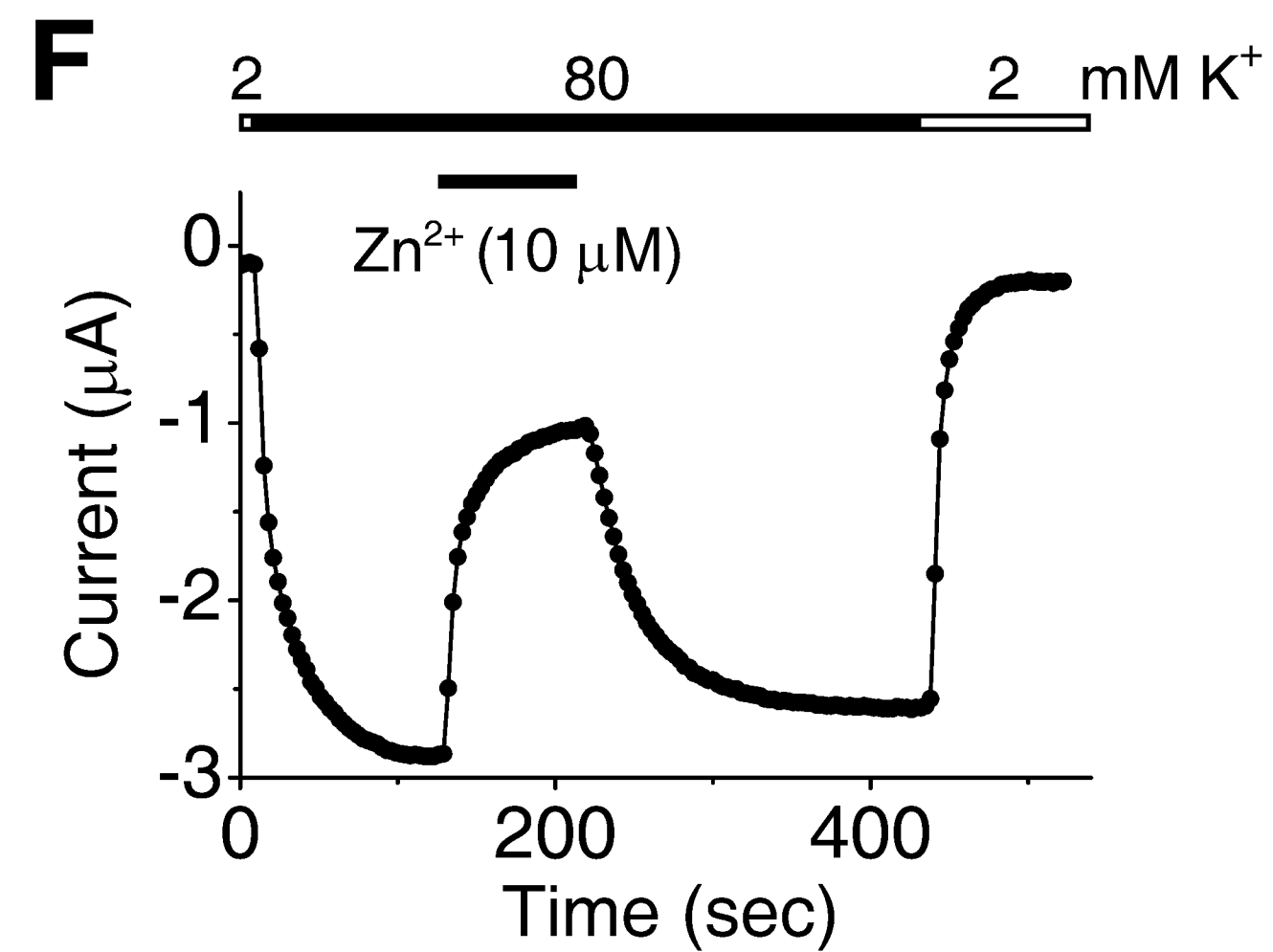
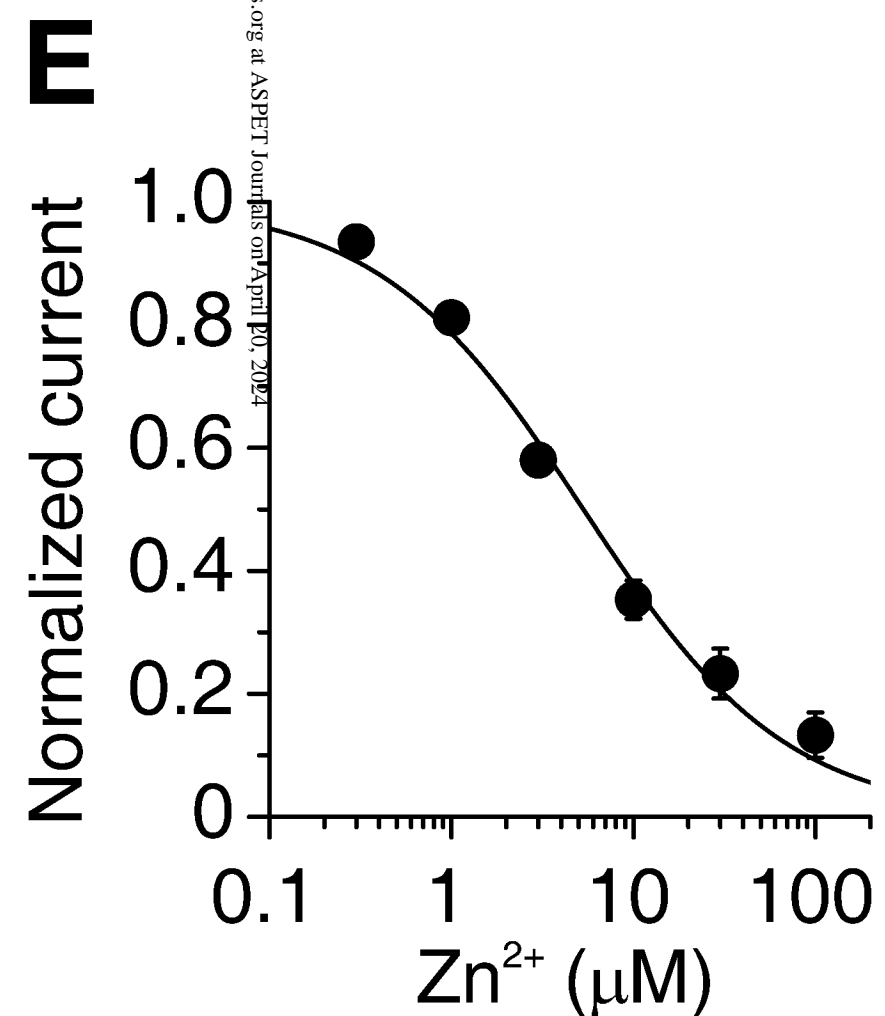
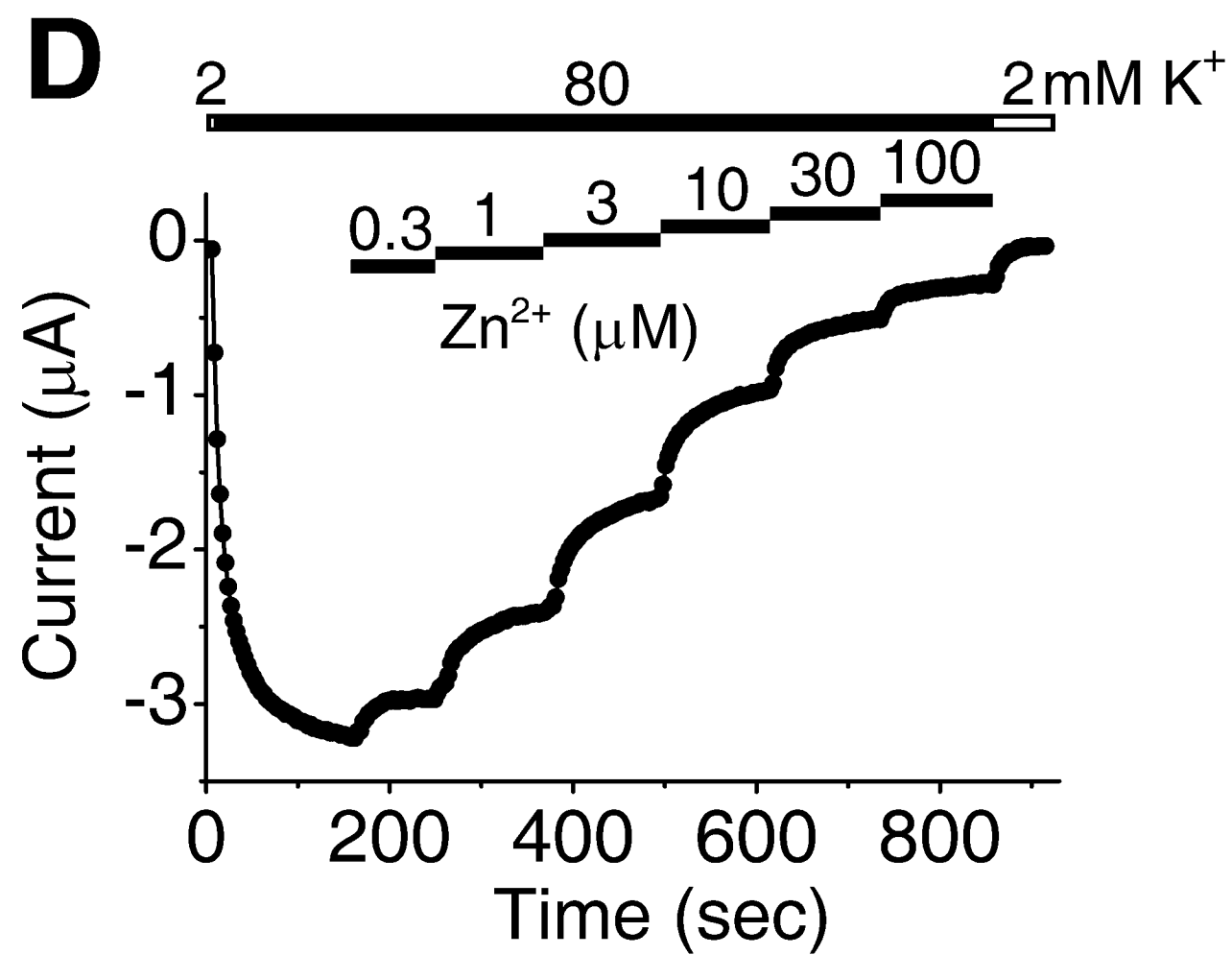
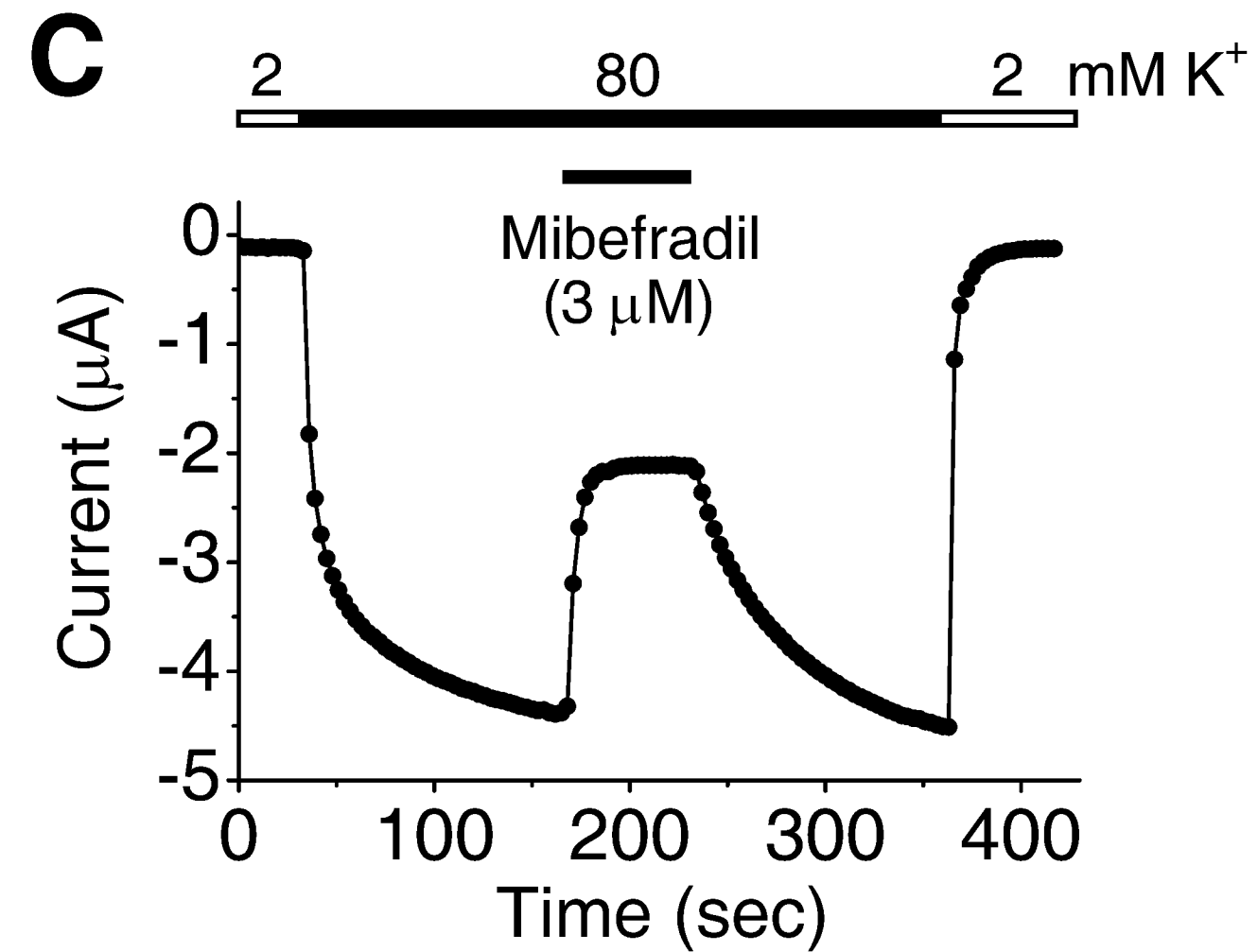
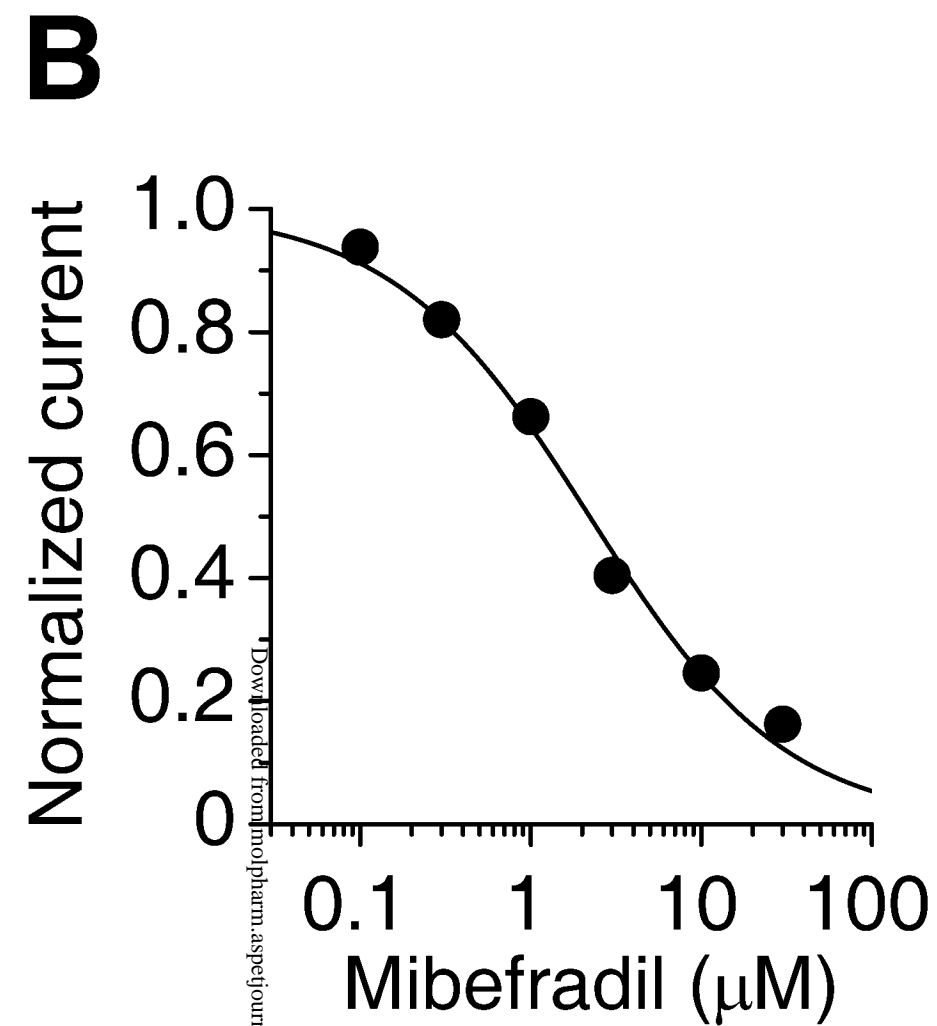
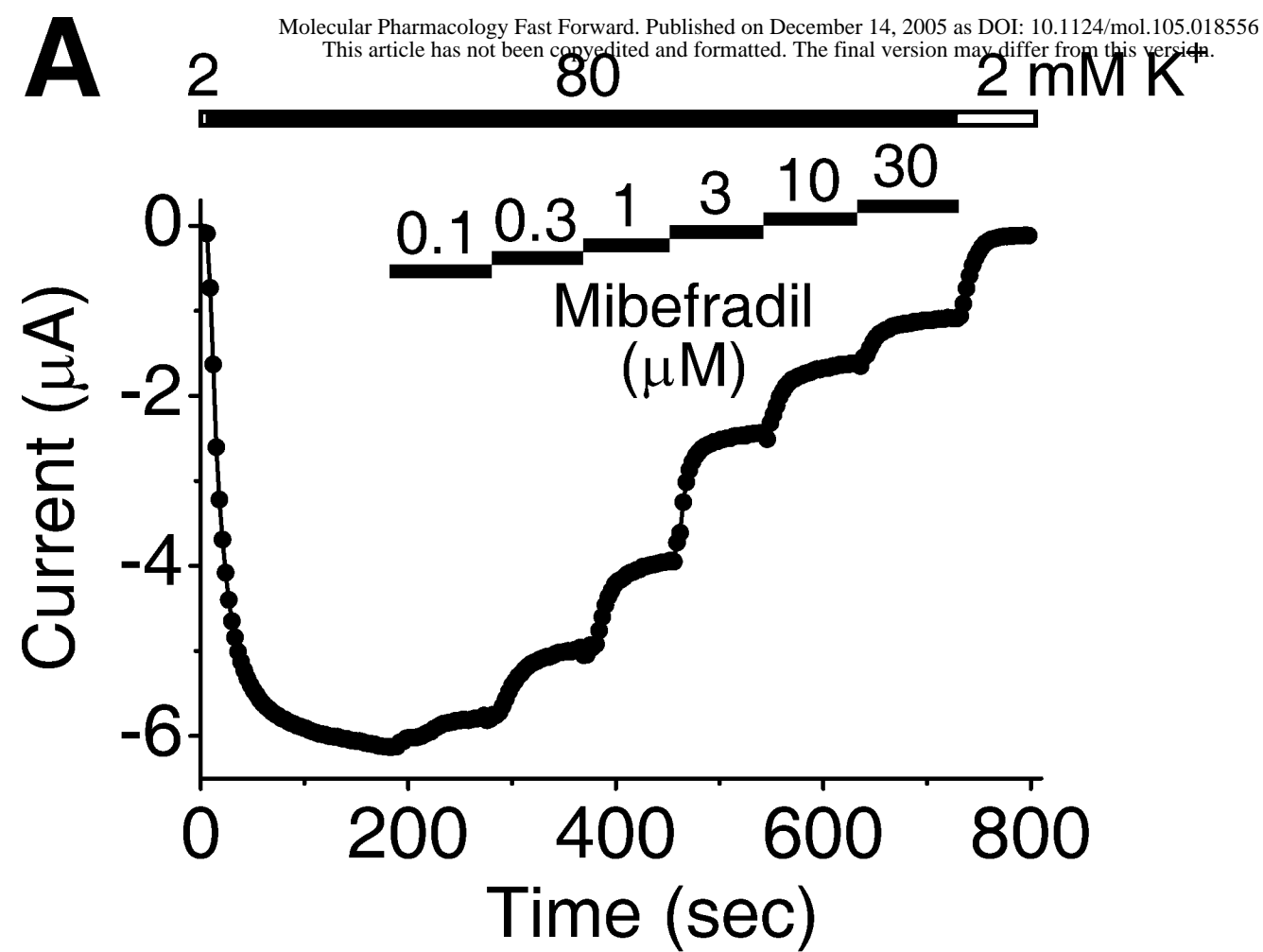
Forward (*upper*) and reverse (*lower*) primers are shown for each channel. The incorporated restriction enzyme sites are marked with lower case letters. The third column contains the annealing temperatures and the number of cycles performed at the given temperature during the PCR amplification.

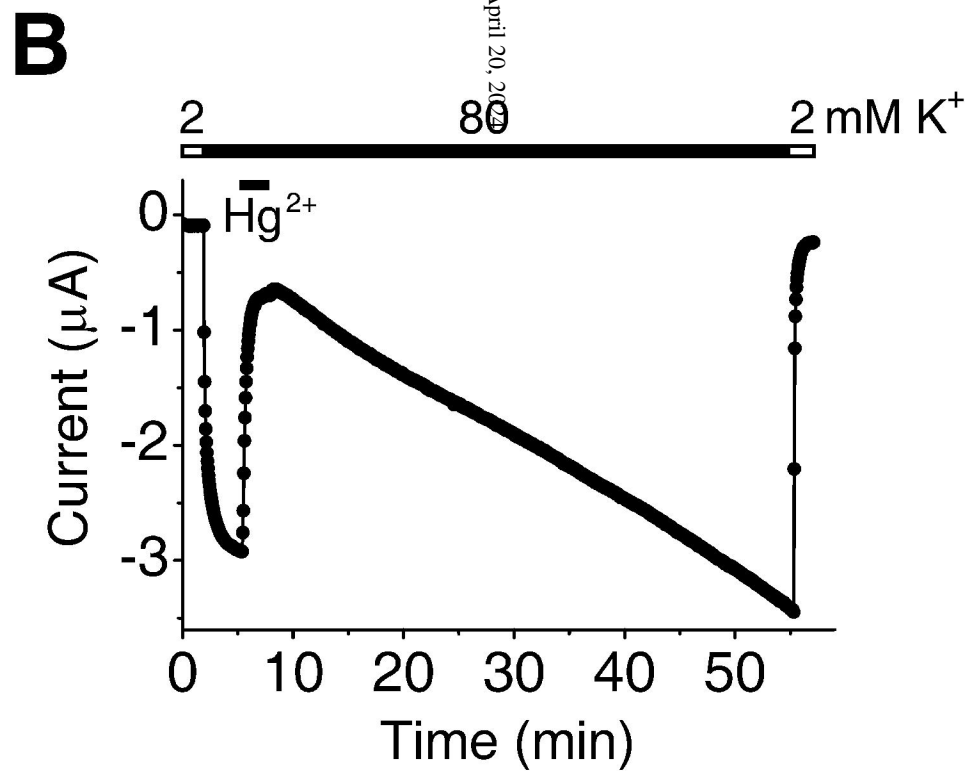
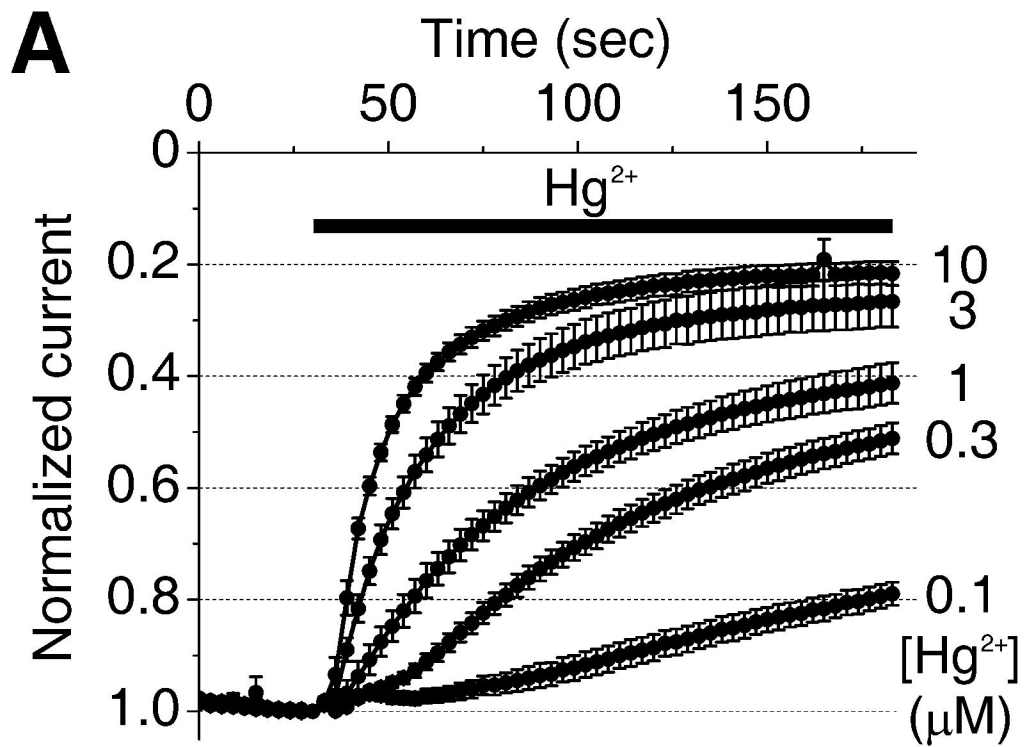
<b>Mutation</b>	<b>Sense oligonucleotide (5' → 3')</b>	<b>Restr. enzyme</b>
C77,82S	CCTGGACGATCTGT <u>cg</u> AACATCCTGAAAT <u>cg</u> AAC CTGACAGTGGTTG	TaqI
C95S	GTAGCAGGAAGAACTT <u>aa</u> GTGAGCATCTGCAAC	Tru1I
C121,122S	CTCTCTTCTTCT <u>Cg</u> T <u>cg</u> ACAGTGTTTCAGCAC	Sall
C329S	GGATGCTTTCTACTT <u>C</u> AGCTTTGTGACtCTGACC ACCATCG	HinI
H132Y, M133I	CAGTGGGTTATGGCT <u>I</u> ACAT <u>C</u> TACCCgGTCACCA GGCTCGG	Eco91I
Y121H, I122M	ACCGTGGGCTATGGC <u>c</u> A <u>t</u> ATgTACCCCGTCACCA GG	NdeI

**Tabl. 2. Oligonucleotide sequences and incorporated restriction enzyme sites for in vitro site-directed mutagenesis of mouse and human TRESK.**

The sense primer sequences are shown for each mutation. The nucleotides changed for altering the amino acid sequence are underlined. Mutations contributing to the new restriction enzyme sites are marked with lower case letters.

# Figure 1.



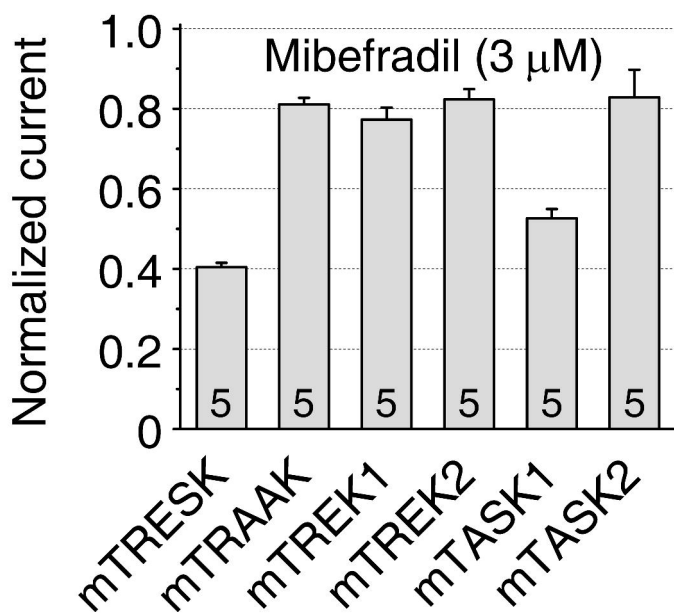
**Figure 2.**



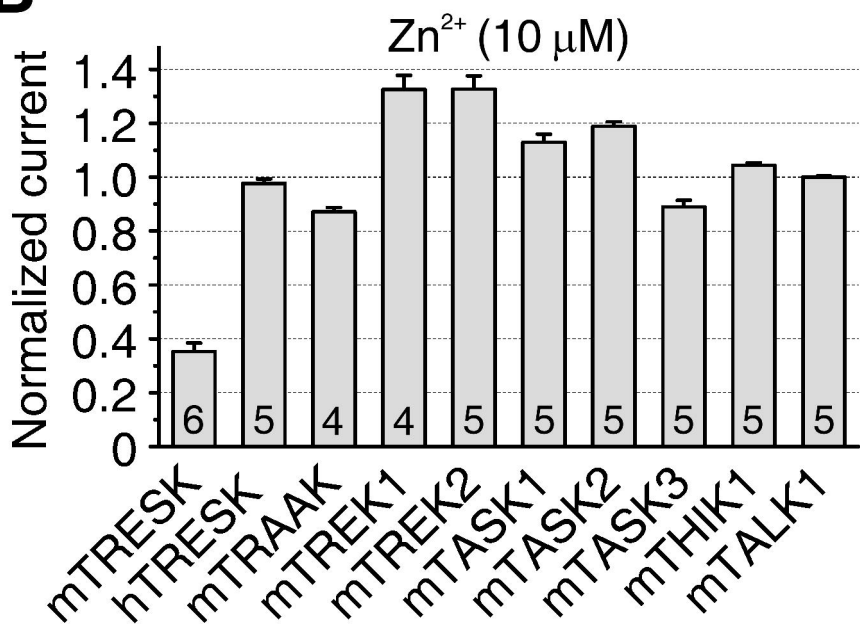
# Figure 3.

Molecular Pharmacology Fast Forward. Published on December 1, 2010. This article has not been copyedited and formatted. The final version of this manuscript may differ from this pre-proof.

## A



## B



## C

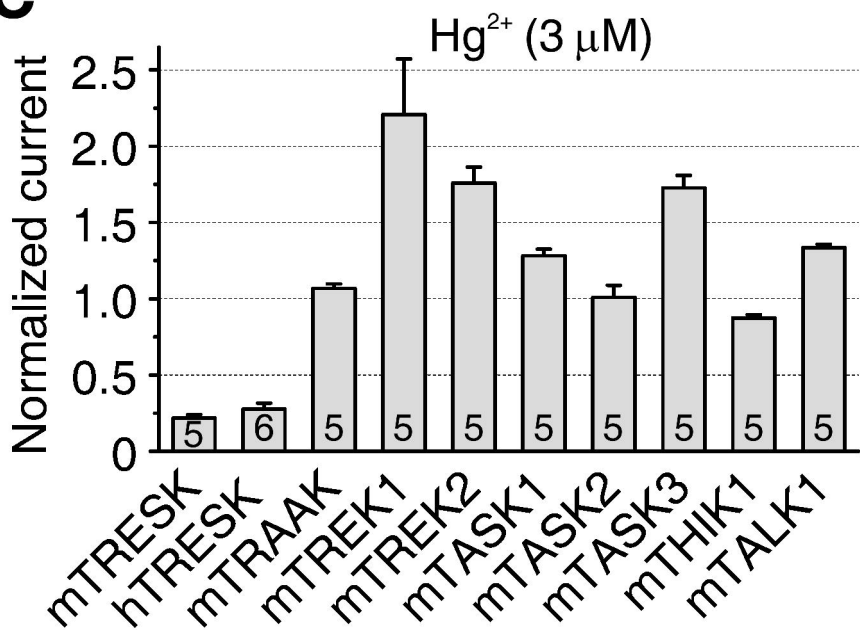


# Figure 4.

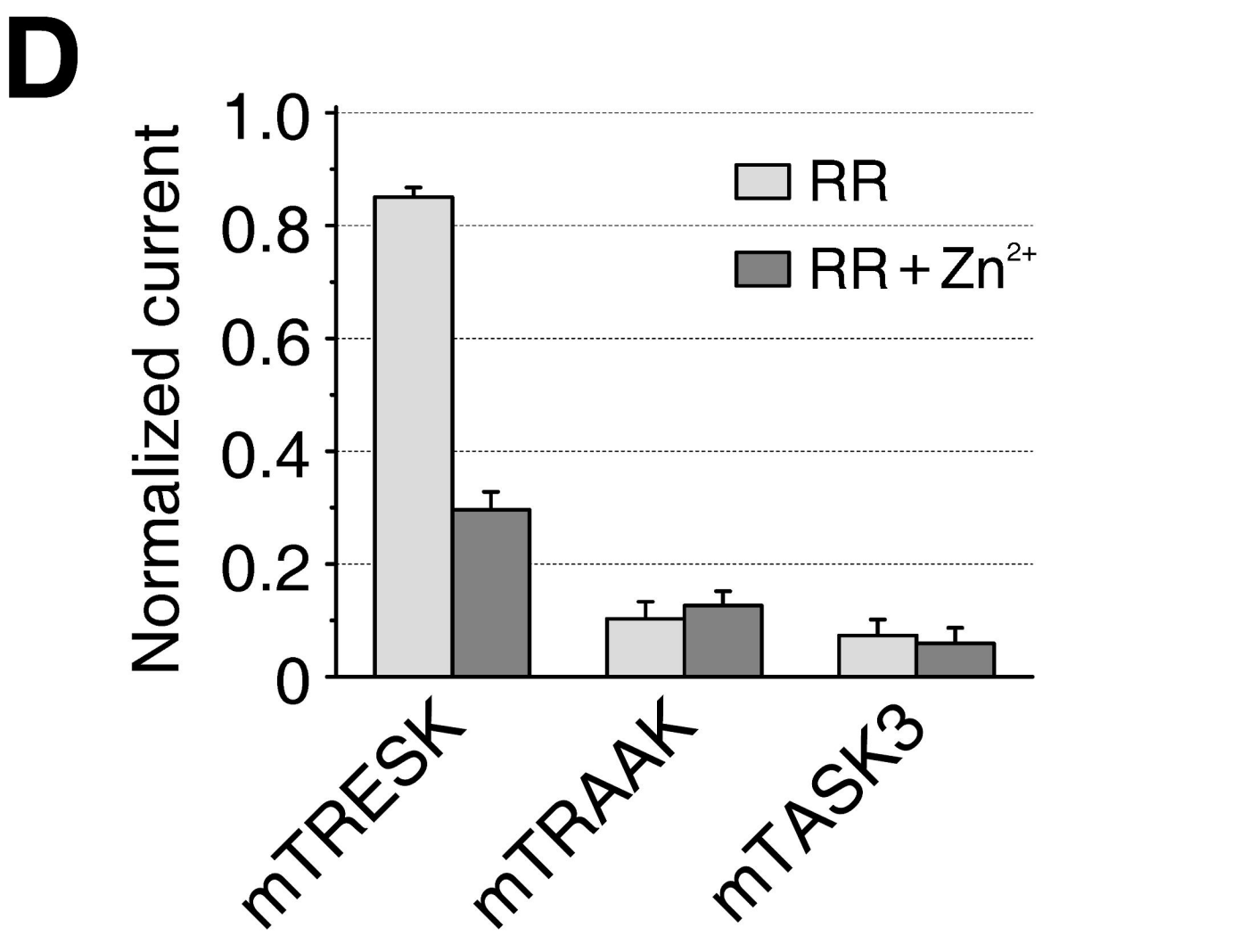
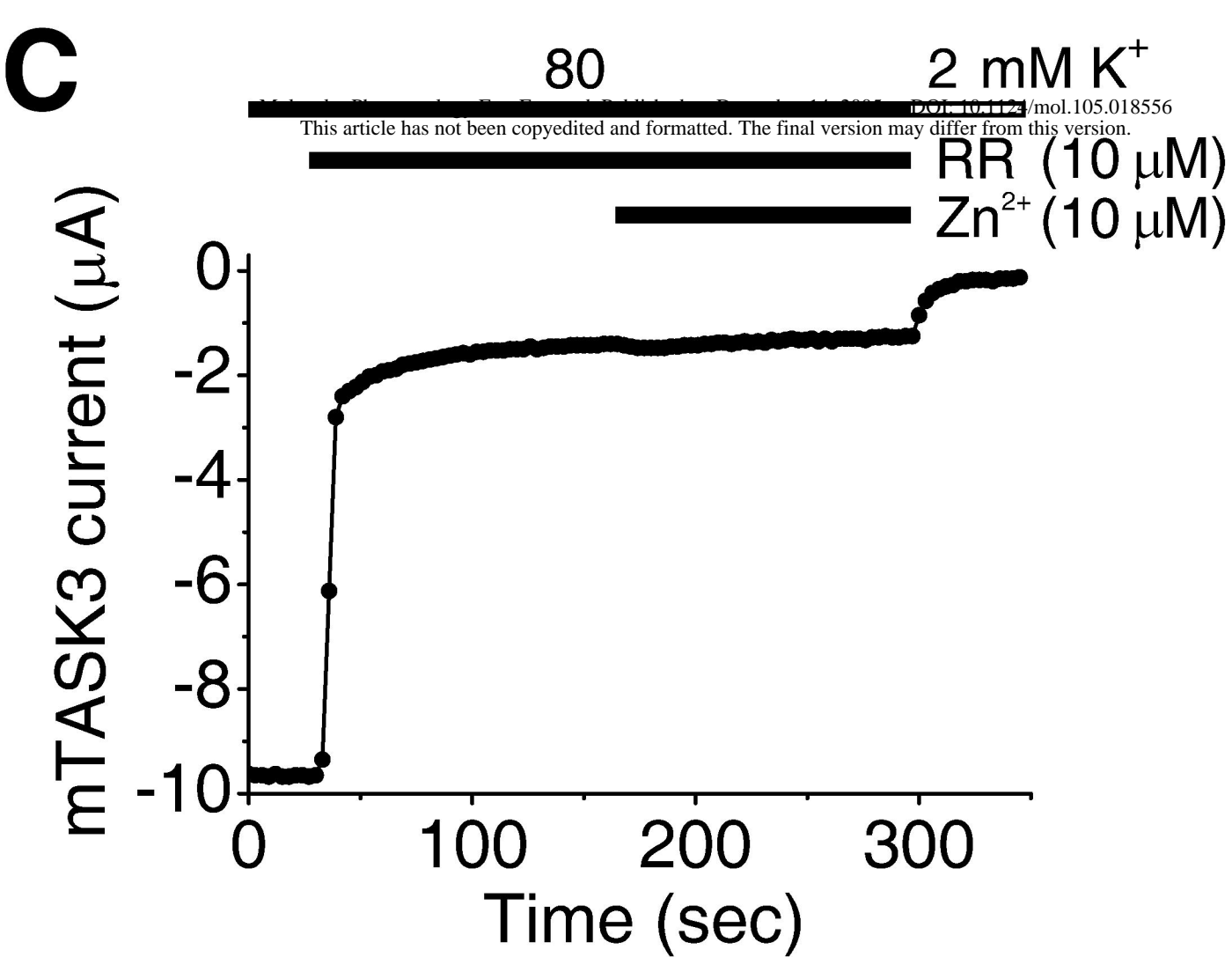
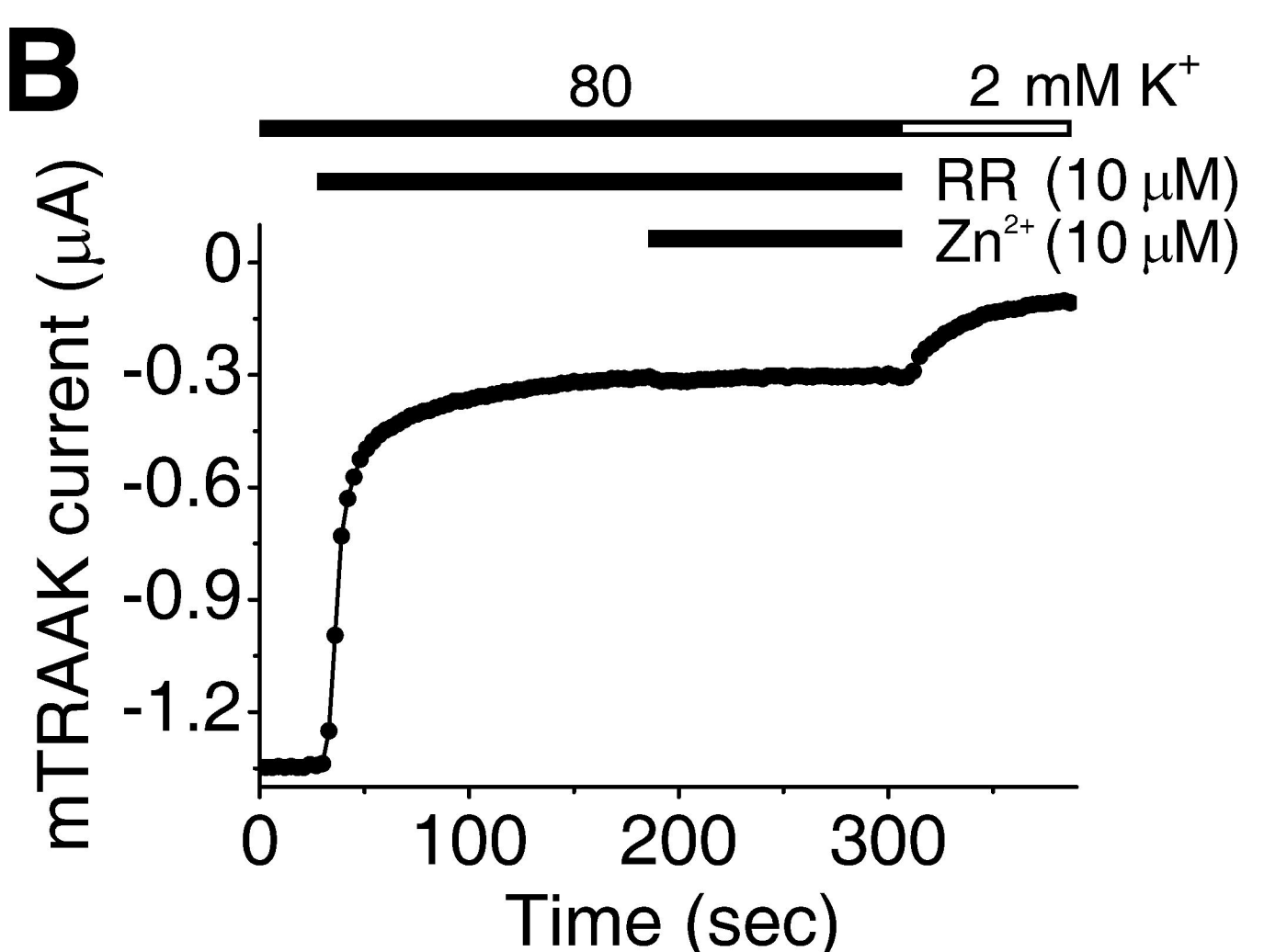
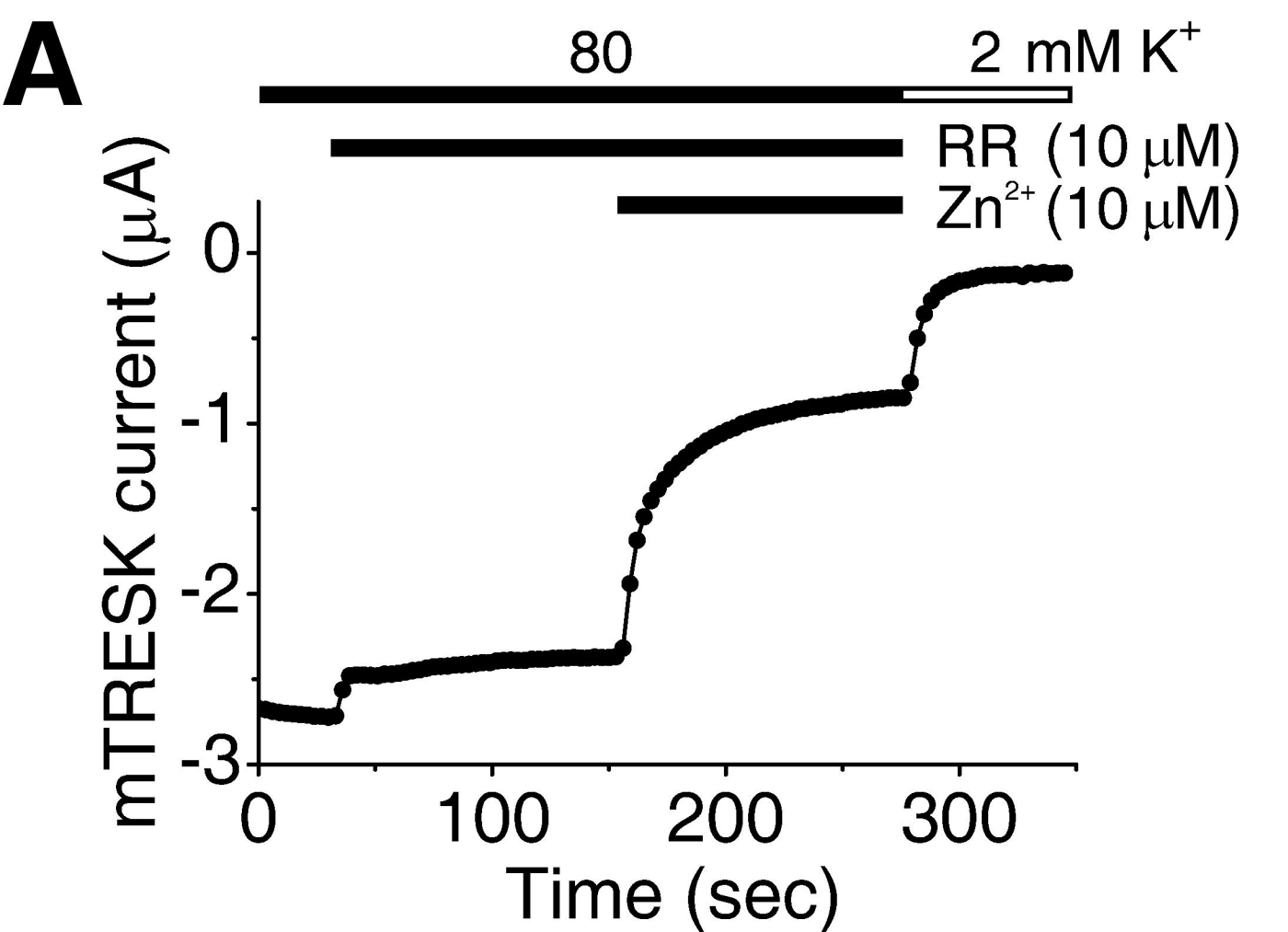


# Figure 5.

Molecular Pharmacology Fast Forward. Published on December 14, 2005 as DOI: 10.1124/mol.105.018556  
This article has not been certified for peer review. The final version may differ from this pre-proof.

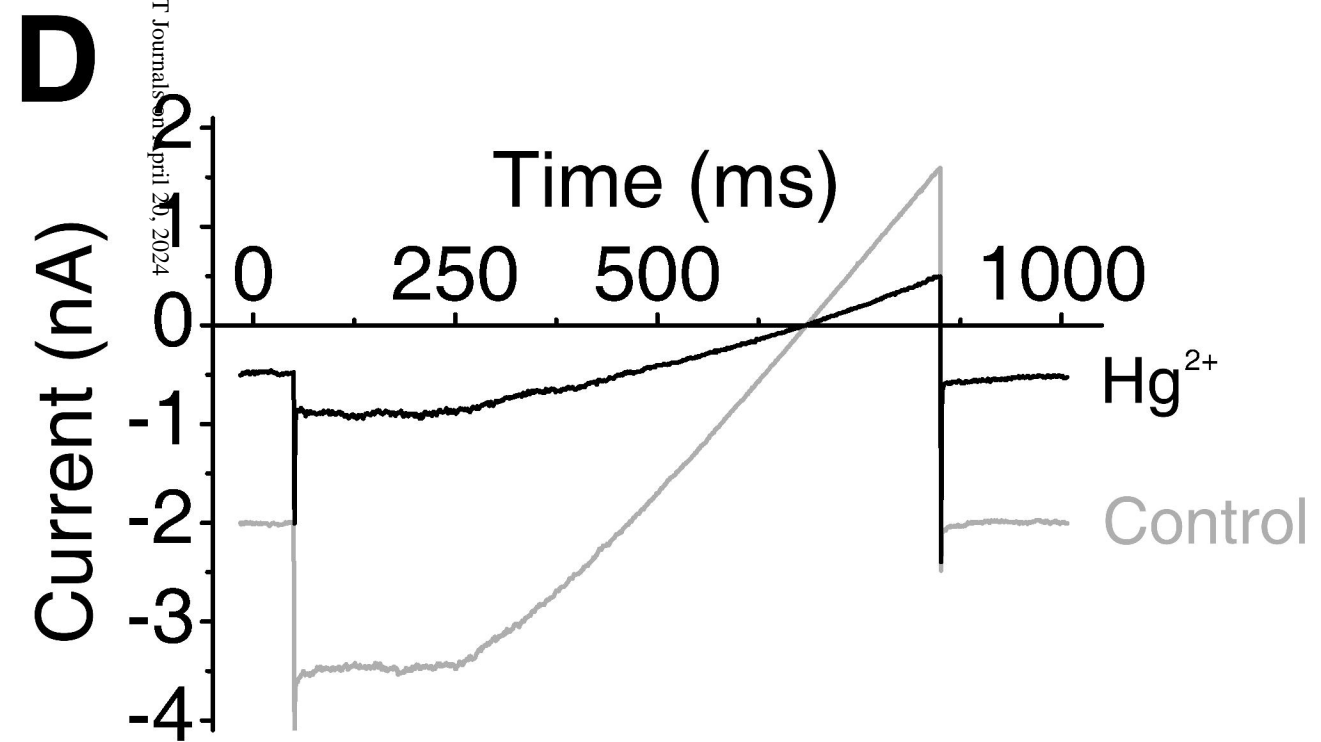
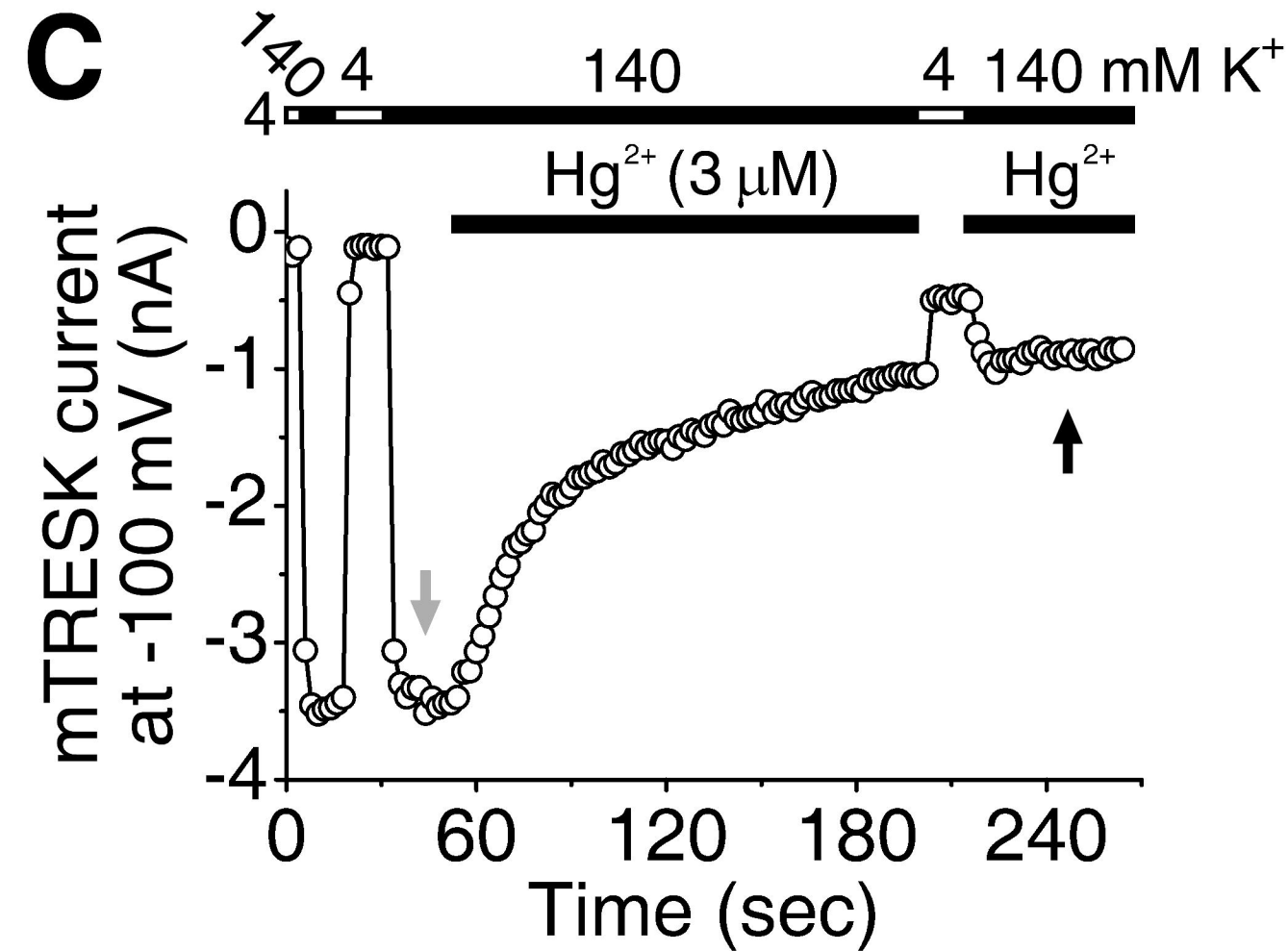
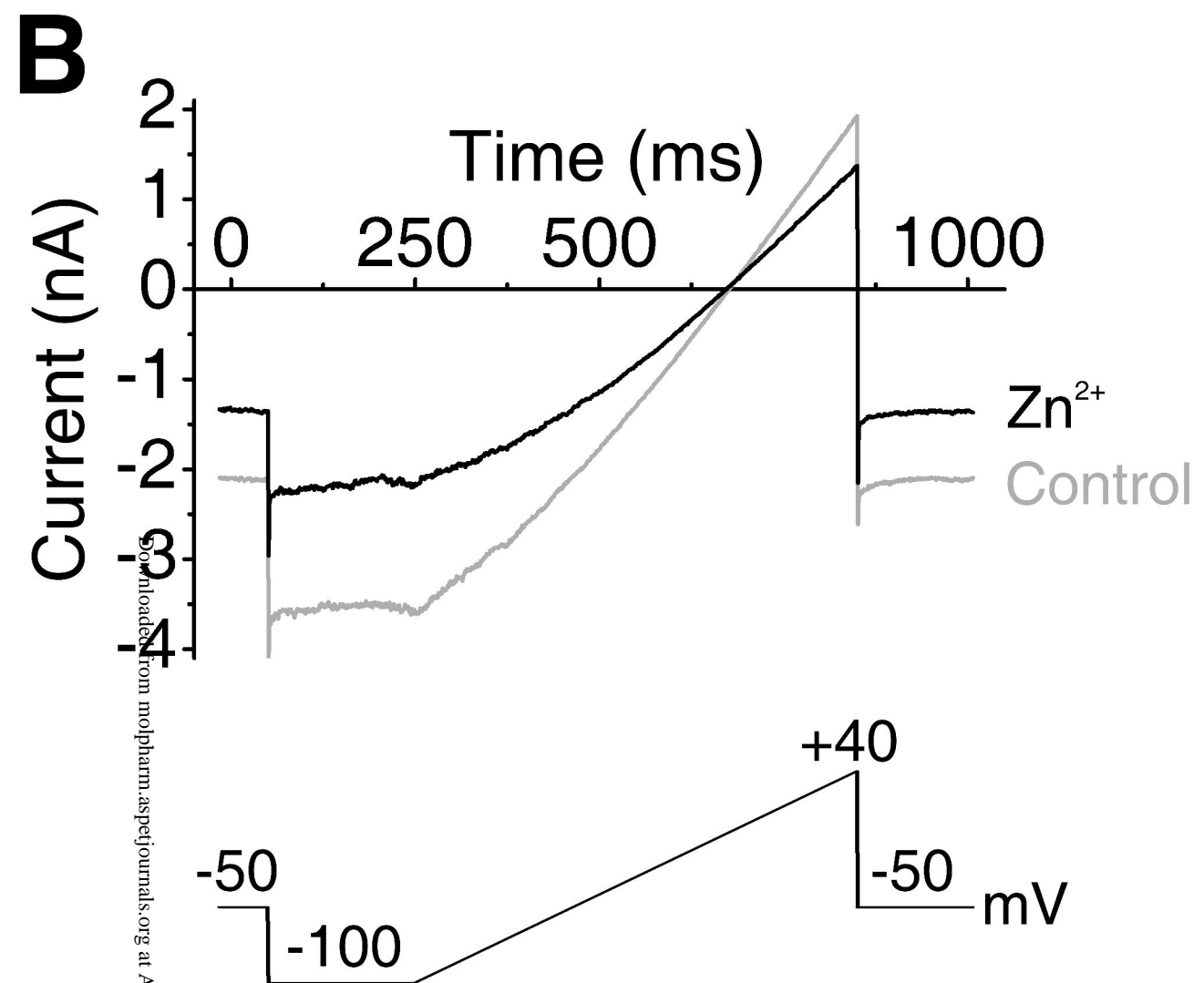
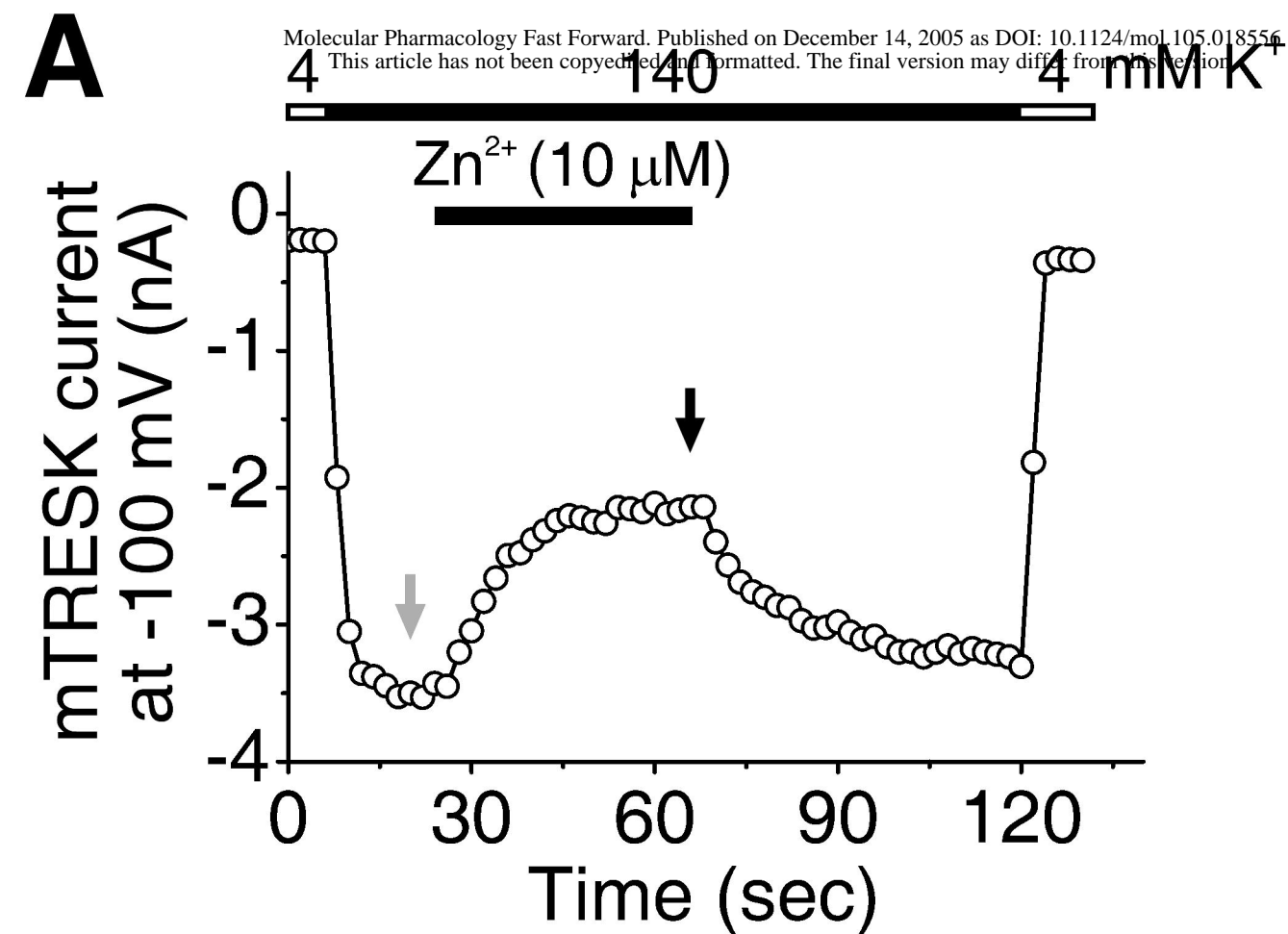


**Figure 6.**

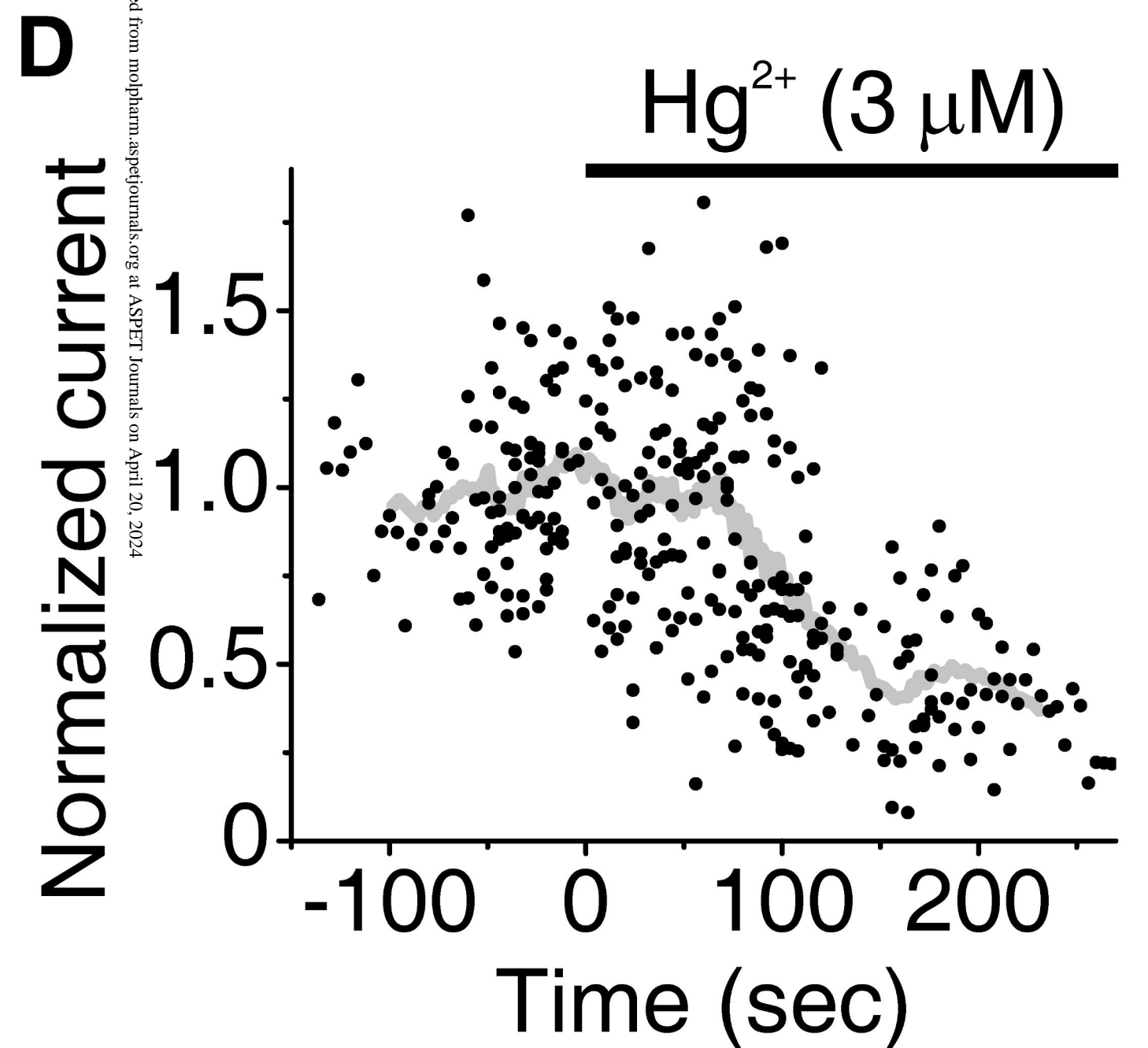
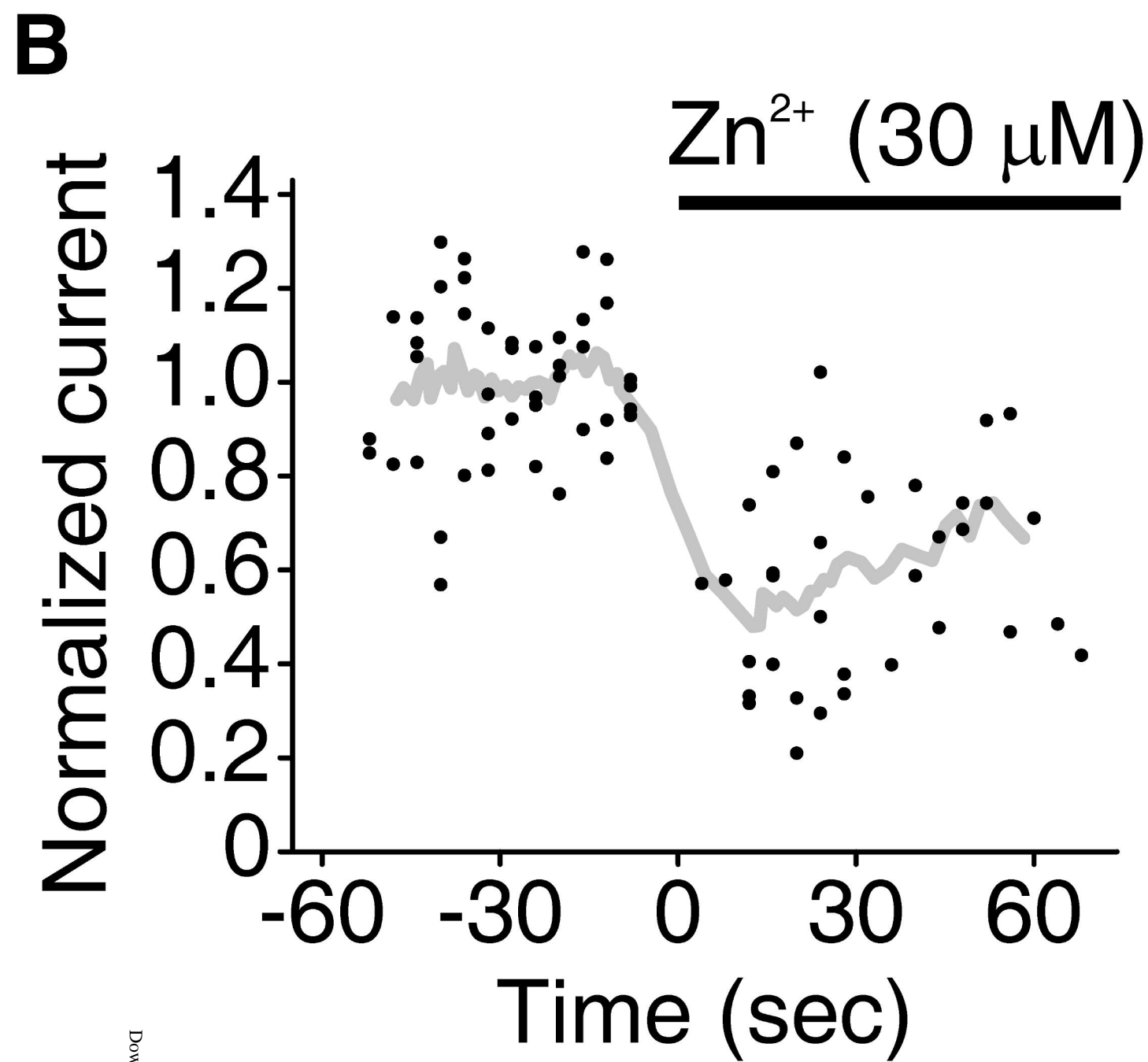
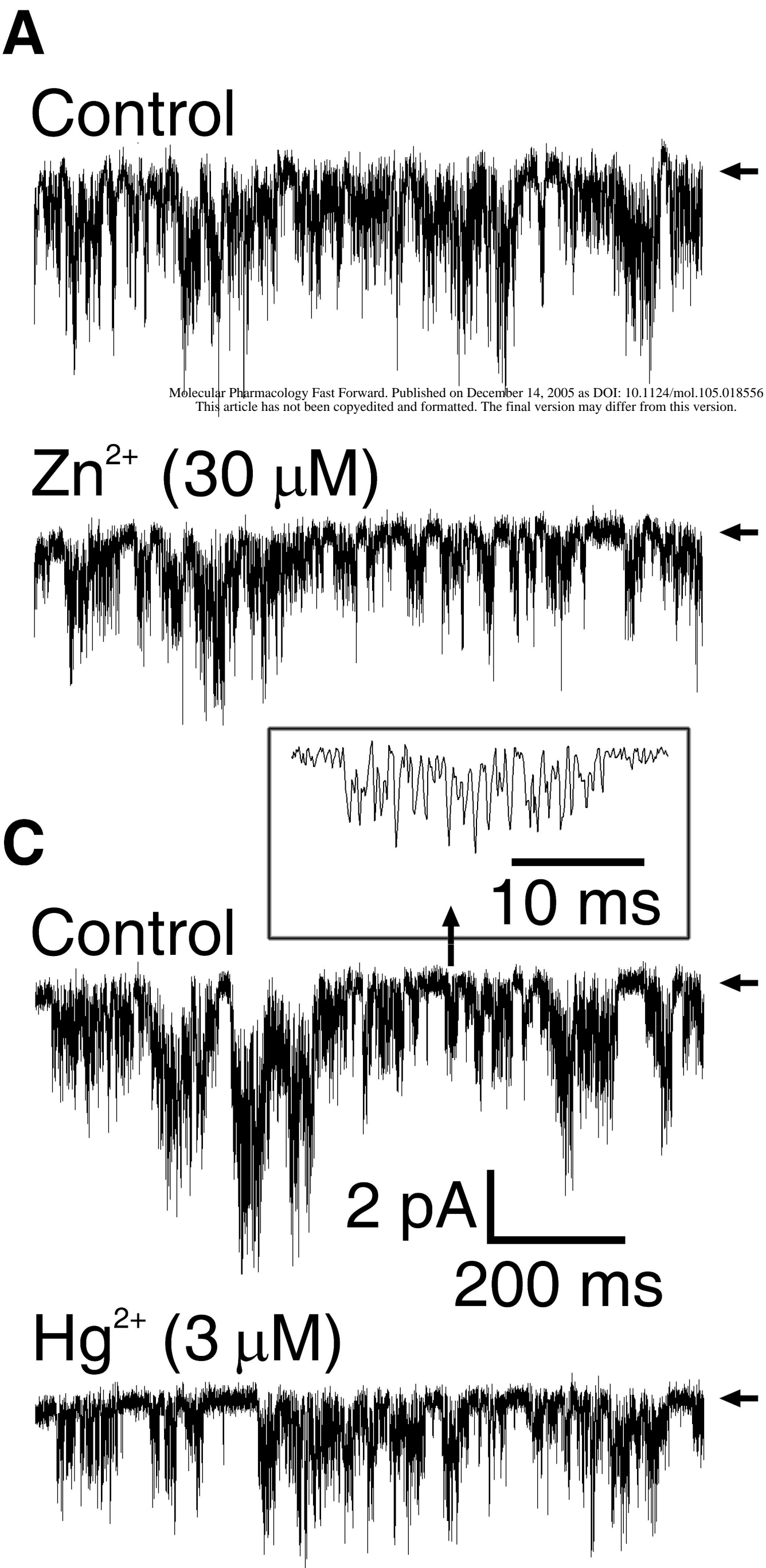
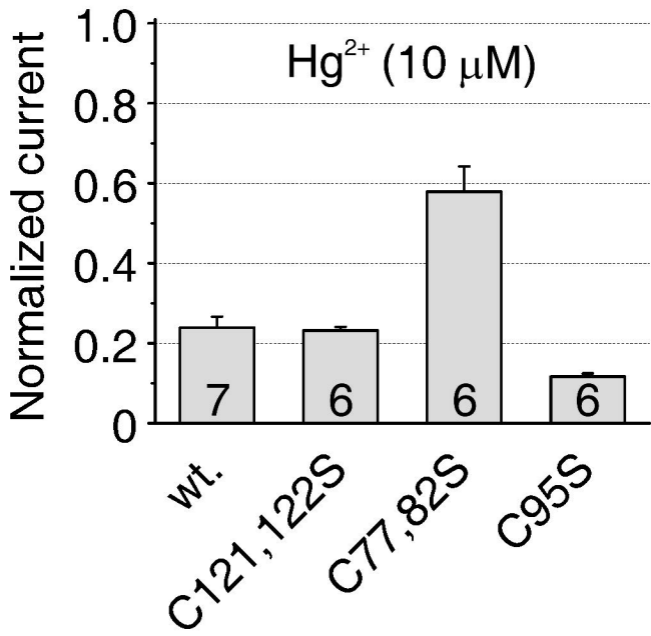


Figure 7.



**Figure 8.**

